Universidade de Aveiro Departamento de Química

2014

Ricardo Jorge Botas Neves dos Santos

Caracterização de sistemas eutéticos constituídos por líquidos iónicos

Characterization of eutectic systems constituted by ionic liquids

Universidade de Aveiro Departamento de Química

2014

Ricardo Jorge Botas Neves dos Santos

Caracterização de sistemas eutéticos constituídos por líquidos iónicos

Characterization of eutectic systems constituted by ionic liquids

Dissertação apresentada à Universidade de Aveiro para cumprimento dos requisitos necessários à obtenção do grau de Mestre em Engenharia Química, realizada sob a orientação científica do Prof. Dr. João Manuel da Costa Araújo Pereira Coutinho, Professor Catedrático do Departamento de Química da Universidade de Aveiro e da Dr[a]. Mara Guadalupe Freire Martins, Investigadora Coordenadora do Departamento de Química, CICECO, da Universidade de Aveiro.

Dedico este trabalho a todas as pessoas que nunca, nem por um momento, deixaram de acreditar em mim e que me incentivaram sempre a continuar a persecução deste sonho.

o júri

presidente

Prof. Dr. Carlos Manuel Santos Silva
professor auxiliar do Departamento de Química da Universidade de Aveiro

Prof. Dr. João Manuel da Costa e Araújo Pereira Coutinho
professor catedrático do departamento de Química da Universidade de Aveiro

Prof. Dr. Luís Manuel das Neves Belchior Faia dos Santos
professor associado da Faculdade de Ciências da Universidade do Porto

Agradecimentos

Gostaria de agradecer a Deus.

Gostaria de agradecer ao Professor Dr. João Coutinho pela oportunidade fantástica que me concedeu de poder desenvolver este trabalho. A sua orientação quer no contexto deste trabalho quer no contexto pessoal, foi simplesmente extraordinária. É um privilégio poder privar com um homem com um caracter tão excecional, um líder inigualável e um cientista incomparável. Para si, o meu muito obrigado pela liberdade que me concedeu e pelos desafios que me colocou, eles fizeram com que eu me apaixonasse deveras por este mundo infinito que são a termodinâmica e os líquidos iónicos.

Gostaria também de agradecer à Dr^{a}. Mara Freire pela oportunidade concedida para poder realizar este trabalho. Consigo aprendi tantas e tantas coisas, entre as quais uma que me ficou na memória que é de facto preciso ter agilidade e rapidez ao mesmo tempo que se é solido e consistente. Obrigado pelo seu exemplo fantástico para mim e para todos os jovens deste país. De facto o seu exemplo de alegria e determinação fazem-me olhar para o futuro com ânimo, acreditando que é possível lutar por aquilo em que acreditamos, aqui em Portugal!

Ao Gui um abraço enorme! A tua contribuição para este trabalho foi essencial e preciosa. Sem a tua ajuda incrível, sem a tua enorme sapiência, sem a tua incansável dedicação, este trabalho não seria possível. Todo o teu contributo enriqueceu de uma forma excecional este trabalho. Obrigado pelas gargalhadas e boa disposição.

Ao Dr. José Esperança um grande reconhecimento pela disponibilidade demonstrada e pela frutuosa colaboração. Sem as mesmas, este trabalho também não seria possível.

Ao companheiro Hugo, pela forma graciosa como me acolheu e como me dedicou muito do seu tempo. Com ele todos os novos desafios foram muito mais estimulantes.

A todo o Path, a todos sem exceção, a todos os que estão, aos que estiveram e aos que estarão, expresso o meu enorme reconhecimento e gratidão. De facto este grupo é a demonstração plena e excecional de que é possível trabalhar e atingir o sucesso dentro de um espirito de alegria e comunhão. Convosco sinto-me bem, convosco sinto que cresço e aprendo em cada conversa, em cada silêncio, em cada gargalhada e em cada lágrima. Sei contudo que, dificilmente encontrarei um sítio, onde trabalhar seja tão agradável, mas lembrar-me-ei sempre com um sorriso dos momentos que partilhei convosco e tentarei reproduzir o vosso espírito de amizade e busca pelo conhecimento em cada sítio por onde eu passe.

A todos os meus amigos, foram e serão sempre um pilar muito importante na minha vida. Sinto-me um homem bafejado pela sorte por ter tantos e tão bons amigos. Obrigado por partilharem comigo tantas alegrias e algumas tristezas. Obrigado por me acolherem e aceitarem tal como sou, com os meus muitos defeitos e algumas virtudes. Obrigado por me incentivarem sempre, a continuar esta caminhada, e auxiliarem em tudo o que esteve ao vosso alcance.

À minha mãe, demonstro aqui minha gratidão eterna. Sem o teu apoio seria impossível ter chegado até aqui! Obrigado pela educação que me concedeste e por me indicares sempre o melhor caminho. Obrigado por teres sempre, algumas vezes mais que eu próprio, acreditado e lutado por este objetivo.

À manica e ao mano Luis um obrigado forte pela vossa força e carinho! Obrigado por estarem sempre ao meu lado em todos os momentos! Obrigado à Meme, essa pessoa maravilhosa que veio ao mundo para me alegrar e tornar a minha vida mais bonita.

À minha querida Avó Alzira pelo teu amor incondicional e por veres sempre o meu lado mais bonito. Ao meu avô Zé, aonde quer que estejas, obrigado pelo exemplo que és para mim, como homem determinado e meigo que foste! Sem a vossa ajuda este objetivo não teria sido cumprido!

Finalmente para ti, meu Amor! Nunca, nenhuma palavra que escreva aqui conseguirá descrever o que o meu coração sente! A ti, que sempre estiveste ao meu lado nos bons e maus momentos expresso a minha gratidão. Obrigado por me concederes toda a tua força inspiradora em cada palavra e gesto. Obrigado por acreditares! Sem ti nunca teria chegado aqui! O teu amor preenche a minha vida! Ao teu lado torno-me melhor! Ao teu lado sou muito mais feliz!

palavras-chave

Lquidos iónicos, equilíbrio sólido-liquido, diagramas de fase, sistemas eutéticos, não-idealidade da fase liquída, microscopia, calorimetria diferencial de varrimento, COSMO-RS

Resumo

O principal objetivo deste trabalho consistiu no estudo do equilíbrio sólido-líquido de misturas binárias constituídas por líquidos iónicos. Os líquidos iónicos utilizados eram compostos por um anião comum, o hexafluorofosfato, e catiões de diferentes naturezas, como os aromáticos imidazólio e piridínio, e os catiões não aromáticos como o pirrolidínio, piperidínio e o tetrabutilamónio e fosfónio. As temperaturas de fusão das misturas e dos componentes puros foram obtidas com recurso a um microscópio ótico com luz polarizada e com uma platina termostatizada acoplada. Além disso, também foi utilizada a técnica de calorimetria diferencial de varrimento (DSC) para obter algumas informações adicionais. Através da avaliação dos diagramas de fase, verificou-se que todas as misturas apresentaram um comportamento eutético, com a exceção de um sistema. Verificou-se também que, na maioria dos casos, este comportamento pode ser bem descrito considerando a idealidade das fases liquida e sólida. Dado que alguns compostos puros estudados apresentam transições sólido-sólido significativas, os termos relativos a estas transições não podem ser desprezados quando efetuamos a modelação dos diagramas de fase. Acreditamos que as semelhanças estruturais entre os compostos utilizados na mistura binária justificam o comportamento ideal da maioria das misturas. Verificámos diferenças substanciais de temperaturas entre a composição eutéctica e o componente puro, e em alguns casos mais de 100 K. Isto significa que através de sistemas eutéticos podemos gerar novos líquidos iónicos a partir de sólidos iónicos.

Alguns sistemas revelaram um comportamento não-ideal. As diferenças estruturais entre os componentes com diferentes comprimentos de cadeia alquílica, e o caracter alifático e a simetria em contraponto com componentes com carácter aromático e assimétrico foram as principais razões encontradas para o desvio do comportamento à idealidade. A não-idealidade da fase líquida foi modelada através da equação de Margules.

O modelo COSMO-RS (COnductor-like Screening MOdel for Real Solvents), um modelo baseado numa combinação de química quântica com cálculos de termodinâmica estatística, foi utilizado para calcular os coeficientes de atividade respeitantes aos sistemas eutéticos estudados. Foi feita a comparação entre os valores calculados pelo modelo e os experimentais. Foram também determinados alguns diagramas sólido-liquido utilizando o modelo COSMO-RS. Os resultados obtidos pelo modelo foram concordantes com os dados experimentais, sobretudo nos sistemas com maior desvio à idealidade, validando assim a potencialidade deste modelo para prever o comportamento de novos sistemas.

O sistema composto por hexafluorofosfato de 1-propil-3-metilpiperidínio e 1-propil-3-metilpirrolídinio revelou um comportamento único, uma solução sólida contínua com a formação de uma liga.

keywords

Ionic liquids, solid-liquid equilibrium, phase diagrams, eutectic systems, liquid phase non-ideality, microscopy, differential scanning calorimetry,COSMO-RS

abstract

The main aim of this work was the study of the solid-liquid equilibrium of binary mixtures composed of ionic liquids. The ionic liquids evaluated were constituted by a common anion, the hexaflourophosphate and different nature cations as the aromatic, imidazolium, pyridinium, non-aromatic as the pyrrolidinium and piperidinium and the tetrabutylammonium and tetrabutylphosponium cations. The melting temperatures of the pure components and their mixtures were obtained by a polarized optical microscope coupled to a controlled temperature stage. Furthermore, Differential Scanning Calorimetry (DSC) was used to obtain additional information. Through the evaluation of the phase diagrams behavior, it was found that all mixtures presented an eutectic-like behavior with the exception of one system. It was found also that in most of the studied examples the eutectic behavior could be well described considering the liquid and solid phases as ideal. For some pure compounds important solid-solid transitions were observed. In the cases of the mixtures formed by these components the contribution terms based on these transitions could not be neglected when modeling the phase behavior. The similarities between mixed components justify the ideal behavior observed for most systems. Reasonable temperatures differences between the eutectic composition and the pure component were found, and in some cases over 100 K, meaning that it is possible to generate new ionic liquids from ionic solids.

Some of the studied systems revealed a mild non-ideal behavior. The structural differences between components composed of different alkyl chain lengths and the aliphatic and symmetrical nature *versus* aromatic and asymmetrical components are the main reasons behind the deviations to the ideal behavior. The non-ideality of the liquid phase was modeled by the Margules equation.

The COSMO-RS (Conductor-like Screening MOdel for Real Solvents), a model based on the combination of quantum chemistry calculations with statistical thermodynamics, was used to calculate the activity coefficients of the studied systems. A comparison was made between the values calculated by the model and experimental data. The solid-liquid phase diagrams of some systems were also calculated by COSMO-RS. The results obtained by the model were consistent with experimental data, especially for the systems with higher deviation from ideality, validating thus the ability of this model to describe the phase behavior of new systems.

The system, composed of 1-propyl-3-methylpiperidinium and 1-propyl-3-methylpyrrrolidium hexafluorophosphate, presented a unique behaviour, a continuous solid solution with a formation of an alloy.

Contents

List of Tables

List of Figures

List of symbols

p_A – Partial vapor pressure of component A (Pa)

p_A^* - Total vapor pressure of A as pure liquid (Pa)

x_A - Mole fraction of component A

μ_A^{id} - Ideal chemical potential of component A in an ideal solution

μ_A^* - Chemical potential of pure component A

R- Universal gas constant (8.314 $J \cdot K^{-1} \cdot mol^{-1}$)

T – Temperature (K)

ΔG_{mix}^{id} – Ideal Gibbs free energy of mixing ($J \cdot mol^{-1}$)

ΔS_{mix}^{id} – Ideal entropy of mixing ($J \cdot mol^{-1}$)

ΔH_{mix}^{id} - Ideal enthalpy of mixing ($J \cdot mol^{-1}$)

X^E – Excess function

V^E – Excess molar volume ($cm^3 \cdot mol^{-1}$)

V_{mix} – Molar volume of the mixture ($cm^3 \cdot mol^{-1}$)

V_{id} - Ideal molar volume of the mixture ($cm^3 \cdot mol^{-1}$)

γ_i^L - Liquid phase activity coefficient of component i

γ_i^S - Solid phase activity coefficient of component i

$T_{fus,i}$ - Melting temperature of component i (K)

$T_{tr,i}$ - Solid-solid transitions temperature of component i (K)

$\Delta_{fus} H_i$ - Fusion enthalpy of component i ($J \cdot mol^{-1}$)

$\Delta_{tr} H_i$ - Solid-solid transitions enthalpy of component i ($J \cdot mol^{-1}$)

$\Delta_{\text{fus}}C_p$ - Heat capacity of component i at the melting temperature ($J \cdot K^{-1} \cdot mol^{-1}$)

z_i - Mole fraction of component I in the solid phase

a_{12} – Binary interaction parameter

σ_T – Uncertainty of temperature (K)

(σ) – Polarizing charge density

$p_S(\sigma)$ - Sigma profile of a solvent

E_{MF} - Electrostatic misfit energy

E_{HB} - Hydrogen-bonding energy

E_{vdW} - van der Waals energy

$\sigma_{acceptor}$ - Polarization charge of a bonding acceptor

σ_{donor} - Polarization charge of a bonding donor

a_{eff} - Effective contact area between two surface segments

α' - Electrostatic misfit interactions parameter

c_{HB} - Hydrogen-bond strength

(σ_{HB}) - Hydrogen-bonding threshold

τ_{vdW} - Specific van der Waals interaction parameters

τ'_{vdW} - Specific van der Waals interaction parameters

$\mu_S^{X_i}$ - Chemical potential for solute X in a liquid S

List of abbreviations

IL or ILs – Ionic liquid or ionic liquids

IL-IL – Ionic liquid-ionic liquid

$[C_nC_1im]^+$ - 1-alkyl-3-methylimidazolium cation

$[C_nC_1C_1im]^+$- 1-alkyl-2,3-dimethylimidazolium cation

$[C_npy]^+$ - *N*-alkylpyridinium cation

$[C_nC_1pip]^+$ - *N*-alkyl-*N*-methylpiperidinium cation

$[C_nC_1pyrr]^+$ - *N*-alkyl-*N*-methylpyrrolidinium cation

$[N_{m,n,o,p}]^+$ - Tetraalkylammonium cation

$[P_{m,n,o,p}]^+$ - Tetraalkylphosphonium cation

$[S_{m,n,o}]^+$ - Trialkylsulfonium cation

$[PF_6]^-$ - Hexafluorophosphate anion

$[NTf_2]^-$ - Bis(trifluoromethylsulfonyl)imide anion

$[BF_4]^-$ - Tetrafluoroborate anion

$[Cl]^-$ - Choride anion

$[Br]^-$ - Bromide anion

$[I]^-$ - Iodide anion

$[OTf]^-$ - Trifluoromethanesulfonate anion

$[C_1CO_2]^-$ - Acetate anion

$[FSI]^-$ - bis(fluorosulfonyl)imide anion

$AlCl_3$ - Aluminium chloride

EtPyBr - ethylpyridinium bromide

SLE – Solid-liquid equilibrium

VLE – Vapor-liquid equilibrium

DES – Deep eutectic solvent

$[C_3C_1im][PF_6]$ - 1-methyl-3-propylimidazolium hexafluorophosphate

$[C_3\ C_1py]\ [PF_6]$ - 1-methyl-3-propylpyridinium hexafluorophosphate

$[C_3C_1pip][PF_6]$ - 1-methyl-1-propylpiperidinium hexafluorophosphate

$[C_3C_1pyrr][PF_6]$ - 1-methyl-1-propylpyrrolidinium

$[C_{12}C_1im][PF_6]$ - 1-dodecyl-3-methylimidazolium hexafluorophosphate

$[N_{4,4,4,4}][PF_6]$ - Tetrabutylammonium hexafluorophosphate

$[P_{4,4,4,4}][PF_6]$ - Tetrabutylphosphonium hexafluorophosphate

$[C_{16}C_1im][PF_6]$ - 1-Hexadecyl-3-methylimidazolium hexafluorophosphate

$[C_{16}py][PF_6]$ - 1-Hexadecylpyridinium hexafluorophosphate

DSC – Differential scanning calorimetry

KF – Karl-Fischer titration

POM – Polarized optical microscopy

CCD – Charge-coupled device

HD – High definition

M_w – Molecular weight

COSMO-RS - COnductor-like Screening Model for Real Solvents

1. General introduction

1.1. Scope and objectives

The high melting temperature of some mesotherms salts, with chemical similarity to ionic liquids but with melting temperatures above 100ºC, excludes them from the ionic liquid realm and also from some applications since high process temperatures are needed for their use. The use of mixtures composed of these salts and also ionic liquids with higher melting temperatures is a promising path to decrease the melting points of these salts by formation of eutectic systems, while maintaining the favorable properties of ILs, such as the low vapor pressure and their aprotic character.[1-2]

The possible number of feasible mixtures between these materials is vast[3], while the number of mixtures composed of ionic liquids, as well as the phase behavior of these systems is still poorly investigated.[4] These facts confirm the pioneering aspect as well as the pertinence of the present work. Furthermore, a profound understanding of these mixtures, and of their phase behavior and properties, can greatly contribute to future improvements on the “designer solvent” concept.

The aim of this work is to generate ionic liquids (from binary mixtures), with melting points lower than room-temperature, from simple mixtures of ionic liquids with higher melting temperatures. Moreover, it is also expected to evaluate the deviations of the liquid phase to the ideal behavior of binary mixtures composed of a range of ionic liquids/mesotherm salts, in particular those formed by a vast number of cations coupled with the hexafluorophosphate anion ($[PF_6]^-$). With this work it is expected to reach a more complete understanding on the chemical interactions occurring between ionic liquids by evaluating the non-ideality of the liquid phase, assessed from the difference between the experimental behavior and the calculated ideal behavior based on the melting profile of the mixture. Additionally, it is also evaluated the predictive ability of COSMO-RS (COnductor-like Screening Model for Real Solvents) for the description of the phase behavior of investigated binary systems.

1.2. Ionic Liquid Definition

Ionic liquids (ILs) could be simply defined as liquids entirely composed of ions[4]; however, this is not so straightforward since the definition itself is a continuous working definition. Usually they can be classified as molten salts, mostly composed of large organic cations with dispersed charge, being the most used cations in synthesis the nitrogen-based, as shown in figure 1. Examples of this family include the 1-alkyl-3-methylimidazolium ($[C_nC_1im]^+$), 1-alkyl-2,3-dimethylimidazolium ($[C_nC_1C_1im]^+$), *N*-alkylpyridinium ($[C_npy]^+$), *N*-alkyl-*N*-methylpiperidinium ($[C_nC_1pip]^+$), *N*-alkyl-*N*-methylpyrrolidinium ($[C_nC_1pyrr]^+$), tetraalkylammonium ($[N_{m,n,o,p}]^+$), and also the phosphonium- and sulphonium-based, as the tetraalkylphosphonium ($[P_{m,n,o,p}]^+$) and the trialkylsulfonium ($[S_{m,n,o}]^+$) cations. The anions can be either inorganic or organic, and the most widespread used are hexafluorophosphate ($[PF_6]^-$), bis(trifluoromethylsulfonyl)imide ($[NTf_2]^-$), tetrafluoroborate ($[BF_4]^-$), choride ($[Cl]^-$), bromide ($[Br]^-$), iodide ($[I]^-$), trifluoromethanesulfonate ([OTf]-), acetate ($[C_1CO_2]^-$), among others. Some examples of the anions chemical structures are depicted in figure 2.

It is a well established, albeit arbitrary, criterion that ILs should present a melting temperature below 373 K. These low melting points can be considered a consequence of the large size of their ions, the unsymmetrical nature of the cation[5], as well as of a delocalized charge[6]. This melting point criterion is based on the boiling point of water and has no physical meaning.[4] For this reason, a large range of mesotherms salts, which are chemically similar to ionic liquids, nevertheless with a higher melting temperature, seem to be rejected from the ionic liquids realm. Regardless of this fact, the reality is that a low melting temperature is an important property which enlarges the *liquidus* domain of these salts, keeping their specific chemical characteristics as ionic substances, and by this, expanding their applicability range while turning them into more useful materials.[7]

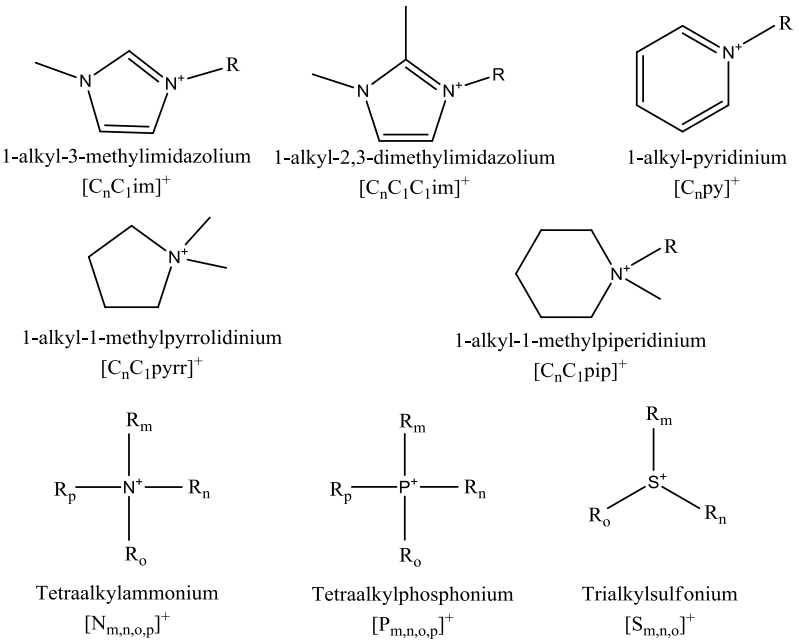

Figure 1 - Common cations used in the synthesis of ionic liquids and their common abbreviations.

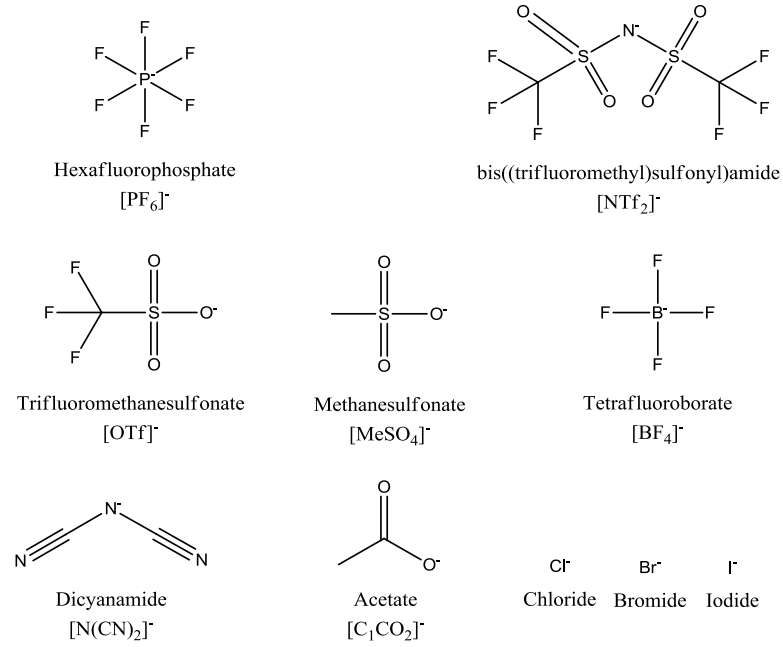

Figure 2 - Most used anions in the composition of ionic liquids and their typical abbreviations.

1.3. Historical view of Ionic liquids

The ionic liquids field started when Paul Walden[8], in 1914, by the neutralization of ethylamine with concentrated nitric acid synthesized the ethylammonium nitrate. This salt presented a melting temperature between 286-287 K, which was a quite unique behavior for a salt, since they normally melt at considerable higher temperatures (for instance, NaCl has a melting temperature of 1074 K). Despite this discovery, not much interest was attributed to this new class of liquids, and only in 1934, Charles Graenacher[9] filled the first patent of an industrial application involving the use of ionic liquids, claiming that halides salts of nitrogen-containing bases were able to dissolve cellulose at temperatures above 373 K.[10] Then, only after the World War II, in 1948, new developments were performed, and another two patents appeared describing the use of mixtures of aluminium(III) chloride and 1-ethylpyridinium bromide for the electrodeposition of aluminium. Later on[11] it was reported the phase diagram of the mixture of aluminium chloride and ethyl pyridinium bromide, as presented in figure 3, showing the lower melting eutectic temperature at a composition of two moles of aluminium chloride ($AlCl_3$) *per* mole of ethylpyridinium bromide ($[C_2py]Br$).[3] Nevertheless, the moisture sensitiveness of these ionic liquids represented a major drawback for their use in industry, which was overcome by the report in 1992, by Wilkes and Zaworotko[12], for the synthesis of water and air stable ILs with the introduction of alternative anions as tetrafluoroborate and nitrate. Moreover, a major advantage in the preparation of these compounds was highlighted since the need of an inert atmosphere box was avoided.

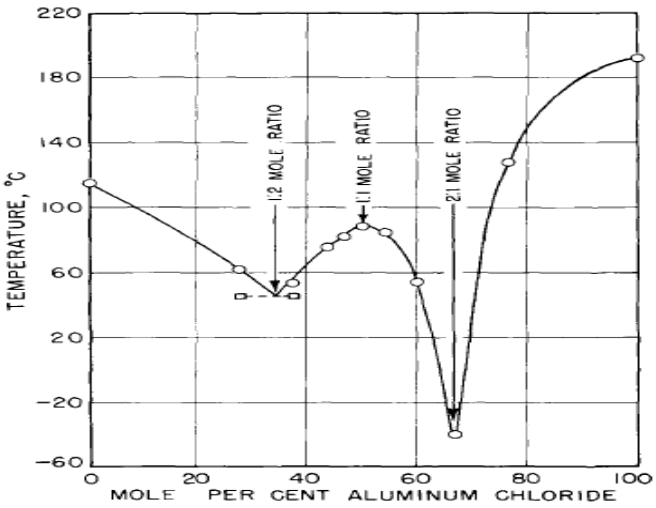

Figure 3 - First solid-liquid phase diagram reported for the system composed of $[C_2py][Br]$ – $AlCl_3$.[11]

In the past few years, the total number of publications dedicated to ionic liquids, either patents or scientific publications, increased almost exponentially and exceeded the 12500 publications in 2013, as shown in figure 4. These amazing records can be explained by the ILs exquisite thermophysical properties, as a negligible volatility, high electrochemical and thermal stability, among many others, and which could explain the great interest that both academia[13] and industry[3] have conceded to these materials.

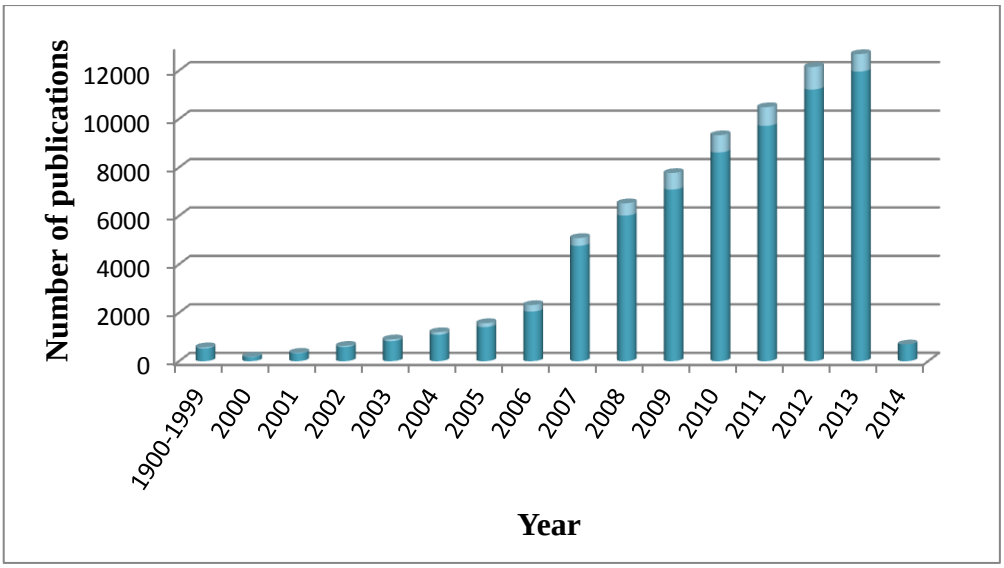

Figure 4 - Number of publications concerning the ionic liquid topic *per* year, patents (light blue) and scientific publications (dark blue). Data taken from Web of knowledge™ with the topic search keywords – "ionic liquid*".[14]

1.4. Designer Solvents Concept

One of the most important features of ILs is their capability as "designer solvents"[15], *i.e*, a proper selection of an anion and a cation allow the tuning of their physical and chemical properties to meet a specific criteria or a specific application[16]. This plethora of possible ionic liquids leads to the creation of novel solvents with designed properties and able to replace the volatile organic solvents currently used, contributing thus to a reduction of the environmental impact while improving safety.[5, 17] The possibility of choosing one cation and one anion, among so many different possible ionic species, opens the possibility to prepare about 10^6 potential new ionic liquids; yet, if one consider their combination into binary systems, or even in ternary systems, the possible new mixtures products are 10^{12} and 10^{18}, respectively, and which means a massive range of new customized applicative-solvents.[3] These numbers are highly appealing when compared with the 600 conventional solvents used in industry and illustrate the broad range of opportunities and the undiscovered world that one still have to unveil in the future. Moreover, the capability of tailor made design products turned ionic liquids into materials with an industrial interest that can take part in the changes of the paradigm of the world industry, building a more sustainable and versatile route of alternative processes.

1.5. Mixtures composed of Ionic liquids

Surprisingly, and despite the fact that until now there are more than 1000 ionic liquids already reported, still a long path has to be made into the ionic liquid mixtures topic.[4,18] Nevertheless, up to present there are already quite promising results reported for binary mixtures of ionic liquids in diverse fields of application, such as in heterogeneous catalysis[19], in the preparation of cellulose nanofibers[20], for improving gas solubility[21], in dye-sensitized solar cells[22-24], as solvent reaction media[25], as gas chromatography stationary phases[26], in biphasic polymerizations[27], in the liquid-liquid extraction of organic solvents[28], in lipids extraction from microalgae[29], and in CO_2 absorption[30] and separation[31]. Furthermore, some works have evaluated, in a theoretical perspective, the IL-IL mixtures by molecular simulations[32-34], their physical properties, such as

densities[35-40], viscosities[1, 36, 38, 40-41], excess volumes[35-36, 40, 42], surface tensions[20,37, 39], vapor pressures[43-45], diffusion coefficients[41], conductivities[36, 46], and surface structures[47] and nanostructures[48]. Also chemical properties were evaluated as probing solute and solvent interactions[49], mutual miscibility[50-51], dielectric measurements[36], optical heterodynedetected Raman-induced Kerr effect spectroscopy (OHD-RIKES)[52], and one of the most important, the phase behavior[1-2, 50, 53-66], which is the main objective of the present work.

Some mixtures present a complex phase behavior; for instance, many simple ionic liquids do not exhibit a clear freezing point and many of them never form a crystalline phase[4]. This pattern can be even more intensified when making mixtures of ionic liquids which lead to the enormous difficulty to acquire the full phase diagrams.[1, 54-56, 59] Most of the studies on solid-liquid phase diagrams display a eutectic-type phase diagrams.[2, 62-63, 67] This type of diagram exhibit an eutectic (from the Greek word ***eutēktos*** *"*easy melting*"*) reaction which as defined by Gamsjäger *et al.*[68], as an isothermal reversible reaction of a liquid phase l which is transformed into two (or more) different solid phases, α and β, during the cooling of a system. In a binary system,

$$I \leftrightharpoons \alpha + \beta$$

where I is a liquid phase, α, β are solid phases, and the forward arrow indicates the direction of cooling. The equilibrium reaction occurs along the eutectic line at the eutectic temperature. At the eutectic composition, the compositions of the liquid and solid phases are equal, and intermediate to the compositions of the solid phase of the system. This means that, in this type of systems, one can mix two ionic solids that at the eutectic composition will present a melting temperature below or close to room temperature, *i.e*, it is possible to generate room temperature ionic liquids from two ionic solids, enlarging therefore the *liquidus* range of the mixture. There are some systems composed of mixtures of ionic and non-ionic components that can exhibit a large depression in the melting temperature, the called deep eutectic solvents (DES) proposed by Professor Abbott[69], and which have received much interest in the past years.[70-72]

1.6. Solid-liquid phase behavior of mixtures composed of Ionic liquids

In 1998, Gordon *et al.*[73], when performing investigations on ionic liquid crystals composed of long alkyl chain lengths and hexafluorophosphate-based salts, studied the effect of mixing two ionic salts, 1-hexadecyl-3-metylimidazolium hexafluorophosphate ($[C_{16}C_1im][PF_6]$) and 1-hexadecylpyridinium hexafluorophosphate ($[C_{16}py][PF_6]$), with the intention of decreasing their melting points without affecting the liquid crystalline temperature range. Curiously, this was a failed attempt on the aim of significant lowering of the melting temperature of the mixture, since contrarily to the authors' expectations, the phase diagram presented a solid solution, showing always a solid phase at temperatures close to room temperature. A recent work carried out by Wang *et al.*[74], aiming at evaluating the mesogenic properties of the binary system composed of 1-dodecyl-3-methylimidazolium tetrafluoroborate ($[C_{12}C_1im][BF_4]$) and 1-dodecyl-3-methylimidazolium iodide ($[C_{12}C_1im][I]$), also presented solid solution phase behavior. Since this aspect was not the focus of these works, there is still a lack on a more profound description and explanation to this solid solution phase behavior.

In 1998, Sun *et al.*[63] published an important study, namely the phase behavior of two binary systems composed of different tetraalkylammonium bis-(trifluoromethylsulfonyl)imide salts. Contrary to the previous cases, the phase diagrams obtained presented eutectic-like phase behavior. Furthermore, some ternary and quaternary mixtures were investigated. Different cations or anions were added to the binary mixture, and it was always found a decrease on their melting temperatures. The authors considered that the effect of the introduction of a new component on the mixture, and thus on the decrease of the eutectic temperature, is independent whether a different cation or anion is introduced into the mixture. The Passerini[53] group reported, for the first time, mixtures composed of *N*-alkyl-*N*-methylpyrrolidinium ($[C_nC_1pyrr]^+$) and lithium cations and a common anion bis(trifluoromethanesulfonyl)imide ($[NTf_2]^-$)[53], and later with two different pyrrolidium-based cations varying the alkyl side chain length and four different types of anions[54], and revealed important improvements on their ionic conductivity

and on the design of new electrolytes for direct application in lithium-based batteries. Later, Bayley and co-workers[61] reported the phase behavior of a binary system composed of two different anions - bis(trifluoromethanesulfonyl)imide ($[NTf_2]^-$) and bis(fluorosulfonyl)imide ($[FSI]^-$) - while keeping the same cation.[61] The authors[61] also studied a ternary system, a so-called reciprocal ternary, combining the prior binary mixture with the addition of $[Li][NTf_2]$. In this study, it was shown that the mixtures have an ideal behavior, but with solid complex forming. It was also demonstrated that the addition of another component to the binary mixture, enlarges the *liquidus* range, mostly due on the entropic effect.[61] Moreover, in 2012, Annat and co-workers[1] also reported an important study where they compared properties of binary mixtures, made of $[C_3C_1pyrr][NTf_2]$ and other ILs, while varying the alkyl chain size within the same cation family, and using different cation cores such as imidazolium and phosponium, and maintaining the pyrrolidinium cation but using a different anion. In this work simple eutectic behaviors were also demonstrated in addition to an immiscibility gap formation and complex crystallization behavior. In 2013, Kick *et al.*[2] reported a solid-liquid diagram of a binary mixture composed of imidazolium–chloride-based ILs, in this case $[C_2C_1im]^+$ and $[C_4C_1im]^+$, where a simple eutectic was observed with an ideal liquid mixture.

1.7. Defining the ionic liquid mixtures nomenclature

The emergence of studies in literature regarding ionic liquids mixtures created a simple new necessity, *i.e*, the need to have a well-defined nomenclature to describe ionic liquids mixtures. Until this moment, no problem was found to name ionic liquids, since they are salts simply composed of one cation $[A]^+$ and one anion $[X]^-$. With the appearance of a more complex system, as for example [A][X] + [B][X], it was found that it is necessary to have a nomenclature, since the usual ionic liquid nomenclature was not suitable to describe these new binary/ternary/quaternary systems. Two different nomenclatures are being used in order to define these new systems, the *constituent* and the *component* nomenclature. [4, 75]

A constituent of a chemical system is any distinct chemical species, such as an individual molecule or an ion that is present in the system; conversely, a component is defined as a chemically independent constituent. As an example, a cation $[A]^+$ can be defined as a constituent but not as a system component, since it is chemically dependent on the anion $[X]^-$. As the name indicates, the *constituent* nomenclature is based upon the number of *constituents*, while the *component* nomenclature is based upon the number of *components* in the product mixture, as described by Welton and co-workers.[1]This information is summarized in table 1. In this work we will adopt the component nomenclature since it is more appropriate in terms of simplicity when facing systems of higher complexity, and is in agreement with previous methodologies (following the molten salts mixtures nomenclature) and semantics if one consider that the product of the mixture is a mixture of ionic liquids[4].

Table 1 - Nomenclature for the mixtures of ionic liquids, and adapted from Niedermeyer *et al.*[4]

Mixture	**Abbreviation**	**No. of Comp.***	**No. of Const.†**	***Comp.* nom.**	**†*Const.* nom.**
None	[A][X]	1	2	Simple	Binary
[A][X] + [A][Y] or [A][X] + [B][X]	[A][X][Y] or [A][B][X]	2	3	Binary	Ternary
[A][X] + [B][Y]	[A][B][X][Y]	2	4	Reciprocal binary	Quaternary
[A][X] + [B][X] + [B][Y] or [A][X] + [A][Y] + [B][Y]	[A][B][X][Y]	3	4	Reciprocal ternary	Quaternary

* Component nomenclature † Constituent nomenclature

1.8. Ideal solutions and thermodynamics of mixing

The first concept that should be considered is the definition of an ideal solution. François Raoult, observed that when doing a sequence of experiments involving mixtures of components with large similarities, the mole fraction of component A in the mixture (x_A) is approximately equal to the ratio between the partial vapor

pressure of component A and the vapor pressure of the pure liquid (p_A/p_A^*). Nowadays, this definition represents the well-established Raoult's law:

$$p_A^{id} = x_A\, p_A^* \quad \textbf{(1)}$$

Therefore, an ideal solution is a liquid mixture that obeys Raoult's law all the way through the complete range of composition from pure A to pure B.[75] However, it is better to define an ideal solution in terms of chemical potential since it implies the Raoult's law instead of stemming from the law itself. Hence, the chemical potential of a component A in an ideal solution is defined as the relation between the chemical potential of pure A (μ_A^*) and the mole fraction of component A in the solution:

$$\mu_A^{id} = \mu_A^* + RT\ ln\ x_A \quad \textbf{(2)}$$

Henceforth, from this definition, it is possible to derive a series of concepts intrinsically related with the thermodynamics of mixing, as the Gibbs energy (ΔG_{mix}^{id}) and the ideal entropy energy (ΔS_{mix}^{id}) of binary mixing described in the following equations:

$$\Delta G_{mix}^{id} = nRT(x_A \ln x_A + x_B \ln x_B) \quad \textbf{(3)}$$

$$\Delta S_{mix}^{id} = nR(x_A \ln x_A + x_B \ln x_B) \quad \textbf{(4)}$$

As a result of the two previous equations, the expression for the ideal enthalpy of mixing (ΔH_{mix}^{id}) can be derived:

$$\Delta H_{mix}^{id} = \Delta G_{mix}^{id} + T\Delta S_{mix}^{id} = 0 \quad \textbf{(5)}$$

This leads us to conclude that in an ideal liquid mixture, all the interactions cancel each other, and as a result, the mixing phenomenon is entropically-driven.

An important parameter which should be considered in order to define ideal solutions and their deviations to the ideality is the activity coefficient (γ). In the presence of an ideal solution, the activity coefficients of all the constituents of the mixture are equal to one. Nonetheless, in the presence of a non-ideal solution, the activity coefficients can present values either superior or inferior to one meaning,

respectively, positive or negative deviations to ideal behavior. It is possible to obtain these activity coefficients either from vapor-liquid equilibrium (VLE) or solid-liquid equilibrium (SLE) data.

Other form of defining deviations to the ideal behavior is to consider thermodynamics *excess functions* (X^E), which is the difference between the measured value and the expected value for an ideal mixture. For instance, excess volume (V^E), an example of an excess function, is defined as the difference between the observed volume of mixing and the ideal volume of mixing as showed in equation 6. The V^E can present positive and negative values which represent positive or negative deviations to ideality.

$$V^E = V_{mix} - V_{id} \quad \textbf{(6)}$$

For instance, Lopes *et al.*[42] described the excess volumes of IL-IL binary mixtures aiming at evaluating the effect of changing the IL cation and anion on the deviations to the ideal mixing behavior. The authors[42] claimed that no significant new interactions appear between the two anions or cations and a constant cation or anion. This pattern means that a quasi-ideal behavior is observed. Nevertheless, with the increase of the difference between the sizes of the cation alkyl side chain, an increase on the non-ideality was observed. This is an expectable trend since with the addition of an IL composed of a cation with a shorter alkyl chain to an ionic liquid composed of a larger alkyl chain length results in the disruption of the dispersive forces.[4]

As mentioned by Niedermeyer *et al.*[4], it is fundamental to learn with previous studies with molten salts on the thermodynamics of mixing, given that the ones regarding IL-IL mixtures have been scarcely reported in literature.[35, 64, 76] Essentially, in these studies[77-78], when the metal complex formation was not observed, an ideal behavior was mostly found. Furthermore, when small negative excess enthalpies of mixing (H^E) were observed, these were attributed mainly to the ions size differences[79], while positive deviations were related to ions with no significant size differences and the deviations were attributed to the changes in the dispersion forces between ions.[80] Small negative excess entropies of mixing

($\Delta_{mix}S^E$) were also found by Kleppla[81], contrarily to what was expected, since up to then it was believed that molten salts had ideal mixing entropies. Negative excess entropies were observed for ionic liquids either with a common anion or with a common cation and they were due to deviations from a random distribution of the ions in solution.[81]

Concerning the excess enthalpy of mixing of ionic liquids, interesting evidences were revealed by Navia *et al.*[35], which can be linked with previous information on the molten salts behavior. Notwithstanding to be possible to consider an overall ideal mixture behavior, two distinct behaviors were observed with small positive and negative excess enthalpies of mixing (H^E).[35] Positive H^E mean a net destruction of interactions between constituents in the mixing process, while negative H^E represent a net creation of interactions. Positive deviations were found in the case of mixtures between ILs with a common anion[35], meaning that interactions between different cations are weaker than the ones between similar cations. Negative excess enthalpies were observed in the case of the mixtures between ILs composed of a common cation and different anions.[35] These results show that the interactions between similar anions are weaker than those between unlike anions.

1.9. **Modeling phase behavior**

In order to model the solid-liquid phase equilibrium, the classical thermodynamic approach reported in literature[82] based on the isofugacity criterion will be adopted herein. From this it is possible, by means of a general simplification based on conventional physicochemical behavior, to characterize the phase behavior of a binary system by equation 7,

$$\ln\frac{x_{\mathrm{i}}\,\gamma_{\mathrm{i}}^{\mathrm{L}}}{z_{\mathrm{i}}\,\gamma_{\mathrm{i}}^{S}}=\frac{\Delta_{\mathrm{fus}}H_i}{R}\left(\frac{1}{T_{\mathrm{fus,i}}}-\frac{1}{T}\right)+\sum_{tr=1}^{n}\left[\frac{\Delta_{tr}H_i}{R}\left(\frac{1}{T_{\mathrm{tr,i}}}-\frac{1}{T}\right)\right]+\frac{\Delta_{\mathrm{fus}}C_p}{R}\left(\frac{T_{\mathrm{fus,i}}}{T}-\ln\frac{T_{\mathrm{fus,i}}}{T}-1\right) \qquad \textbf{(7)}$$

where the mole fraction of liquid and solid state are respectively, x_{i} , and z_{i} , the activity coefficients of component *i* in the liquid and solid state are, respectively, $\gamma_{\mathrm{i}}^{\mathrm{L}}$

γ_i^S, the melting temperature is $T_{fus,i}$ (K), the melting enthalpy is $\Delta_{fus}H_i$, the solid-solid transitions temperature and enthalpy are $T_{tr,i}$ (K), and $\Delta_{tr}H_i$ (J·mol^{-1}), and the heat capacity is $\Delta_{fus}C_p$ (J·K^{-1}·mol^{-1}) at the melting temperature $T_{fus,i}$. Additionally, there is the universal gas constant (R = 8.314 J·K^{-1}·mol^{-1}) and the melting temperature of the mixture is represented by T (K).

For an eutectic system the solid phase is formed by two immiscible solids, and the product between the solid mole fraction and activity coefficient is equal to one. Additionally, another simplification is possible as one can neglect the term containing the heat capacity, $\Delta_{fus}C_p$, since the error introduced is small, if the temperature $T_{fus,i}$ and T are not far apart and considering that the enthalpy-related terms are dominant over the heat capacity term, meaning that the absolute value of the heat capacities are lower than the enthalpies.[83-84] If one can consider the ideality of the liquid phase, which means a liquid activity coefficient equal to one, the following equation can be used to describe the ideal solid-liquid phase behavior:

$$\ln x_i^{id} = \frac{\Delta_{fus}H_i}{R}\left(\frac{1}{T_{fus,i}} - \frac{1}{T}\right) + \sum_{tr=1}^{n}\left[\frac{\Delta_{tr}H_i}{R}\left(\frac{1}{T_{tr,i}} - \frac{1}{T}\right)\right] \quad \textbf{(8)}$$

The activity coefficient, γ_i^L, can be estimated based on these simplification from the differences between equations 8 and 9, *i.e*, the differences between the estimated ideal behavior and the experimental one.

$$\ln \gamma_i^L = \left|\ln x_i^{id} - \ln x_i^{exp}\right| \quad \textbf{(9)}$$

In order to model moderately non-ideal behavior of binary mixtures, the two- and three-suffix Margules equations give good results while they are mathematically easier to handle. In the case of the two-suffix Margules equation, it is only applied for simple mixtures where components are similar in chemical nature and

molecular size.[85] In equation 10 and 11 we depicted the two and three-suffix Margules equations, respectively.

$$RT\ ln\gamma_1 = Ax_2^2 \text{ and } RT\ ln\gamma_2 = Ax_1^2 \quad \textbf{(10)}$$

$$RT\ ln\gamma_1 = (A + 3B)x_2^2 - 4Bx_2^3 \text{ and } RT\ ln\gamma_2 = (A - 3B)x_1^2 - 4Bx_1^3 \quad \textbf{(11)}$$

1.10. COSMO-RS (COnductor-like Screening MOdel for Real Solvents)

In order to validate a tool that could allow the forecasting of the phase behavior and the deviation from ideality of the IL-IL systems, COSMO-RS (COnductor-like Screening MOdel for Real Solvents) was used.

COSMO follows a quantum chemical approach combined with statistical thermodynamics calculations. The quantum chemical basis is a dielectric continuum model.[86-88] This model is able to predict the phase behavior and thermophysical properties of real solvents (RS). This model allows calculations without having any previous knowledge on experimental data, and only based on the properties of each atom that composed a molecule or ion. COSMO calculations are performed in the un-scaled, *i.e.,* an ideal/perfect conductor interface. This virtual conductor environment surrounds the molecules, considering interactions on the electrostatic screening and back-polarization of the solute molecule. All the information that characterizes the electron density and geometry and screening charge density (σ), at a minimum energetic state of the conductor, a reference state, is stored at the so-called COSMO files. The description of the molecular interactions is attained by a σ-profile, $p_S(\sigma)$, a distribution function, which provide the complete description of the molecule.

COSMO also considers three different specific interactions energies, the electrostatic misfit energy (E_{MF}), the hydrogen-bonding energy (E_{HB}) and van der Waals energy (E_{vdW}). The two first energies are a function of the polarization

charges of the two interacting segments (σ,σ') or $(\sigma_{acceptor},\sigma_{donor})$. The following equations describe these three energies:

- electrostatic misfit energy:

$$E_{MF}(\sigma,\sigma') = a_{eff}\frac{\alpha'}{2}(\sigma+\sigma')^2, \quad \textbf{(12)}$$

- hydrogen-bonding energy:

$$E_{HB} = a_{eff}c_{HB}\min(0;\min(0;\sigma_{donor}+\sigma_{HB})\times\max(0;\sigma_{acceptor}-\sigma_{HB})) \quad \textbf{(13)}$$

- van der Waals energy:

$$E_{vdW} = a_{eff}(\tau_{vdW}+\tau'_{vdW}). \quad \textbf{(14)}$$

where a_{eff} is the effective contact area between two surface segments, α' is an interaction parameter, c_{HB} is the hydrogen-bond strength, (σ_{HB}) is the threshold for hydrogen-bonding, and τ_{vdW} and τ'_{vdW} are element specific van der Waals interaction parameters.

Through the following equations (15 and 16), it is possible to calculate the *σ*-potential $\mu_S(\sigma)$ and the pseudo-chemical potential of the component X_i in a solvent S, $\mu_S^{X_i}$. This permits to predict thermodynamic properties and phase behavior, such as the activity coefficients (equation 17).

$$\mu_S(\sigma) = -\frac{RT}{a_{eff}}\ln\left[\int p_S(\sigma')\exp\left(\frac{1}{RT}\left(a_{eff}\mu_S(\sigma') - E_{misfit}(\sigma,\sigma') - E_{HB}(\sigma,\sigma')\right)\right)d\sigma'\right] \quad \textbf{(15)}$$

$$\mu_S^{X_i} = \mu_{C,S}^{X_i} + \int p^{X_i}(\sigma)\mu_S(\sigma)d\sigma \quad \textbf{(16)}$$

$$\gamma_S^{X_i} = \exp\left\{\frac{\mu_S^{X_i} - \mu_X^{X_i}}{RT}\right\} \quad \textbf{(17)}$$

In this work, all the calculations were preformed assuming the electroneutral mixture approach, treating separately each cation and anion in COSMO-RS calculations. Moreover, the conformers used in these calculations were the ones of lower energy, that according to Freire *et al.* [89] is the most accurate approach. The quantum chemical COSMO-RS calculations were carried out in the Turbomole program package[90] with the BP density functional theory, giving the

surface charge density and the Ahlrichs-TZVP (triple-ζ valence polarized large basis set).[91] The activity coefficients, solid-liquid equilibrium diagrams and excess properties were estimated employing the COSMOtherm program using the parameter file BP_TZVP_C2.1_1301.

COSMO-RS has been widely used as a tool for forecasting thermodynamics properties of ionic liquids and phase behavior. COSMO-RS as also been used as a screening tool to evaluate the plethora of ionic liquids for a specific application, as for example for thiols desulfurization.[92] Moreover, as showed by Freire *et al.*[89, 93], COSMO-RS model yields good predictions, either quantitative or, qualitative trends on the LLE and VLE of binary mixtures composed of ionic liquids with alcohols[89] or water[93]. It was also shown that COSMO-RS can reasonable predict the liquid-liquid phase behavior of IL-IL mixtures.[50, 94] Solid-liquid equilibria of mixtures composed of ILs-thiophenes, IL-alcohols and IL-hydrocarbons[95] predicted by COSMO-RS have also been reported. To the best of our knowledge, there has been no previous report on the evaluation of the solid-liquid phase behavior of IL-IL mixtures.

2. Experimental section

2.1. **Materials**

In this work, seven different pure ionic liquids for the preparation of the binary mixtures were used. They are 1-methyl-3-propylimidazolium hexafluorophosphate, $[C_3C_1im][PF_6]$, 1-methyl-3-propylpyridinium hexafluorophosphate, $[C_3C_1py][PF_6]$, 1-methyl-1-propylpiperidinium hexafluorophosphate $[C_3C_1pip][PF_6]$, 1-methyl-1-propylpyrrolidinium hexafluorophosphate $[C_3C_1pyrr][PF_6]$, 1-dodecyl-3-methylimidazolium hexafluorophosphate $[C_{12}C_1im][PF_6]$, tetrabutylammonium hexafluorophosphate $[N_{4,4,4,4}][PF_6]$, and tetrabutylphosphonium hexafluorophosphate $[P_{4,4,4,4}][PF_6]$. The chemical structures of the ionic liquids investigated are depicted in figure 5. All ionic liquids were purchased from IoLiTec company (Heilborn), with the exception of $[N_{4,4,4,4}][PF_6]$ and $[P_{4,4,4,4}][PF_6]$, purchased from Apollo Scientific (Bredbury, UK) and Fluka (Buchs, Switzerland), respectively.

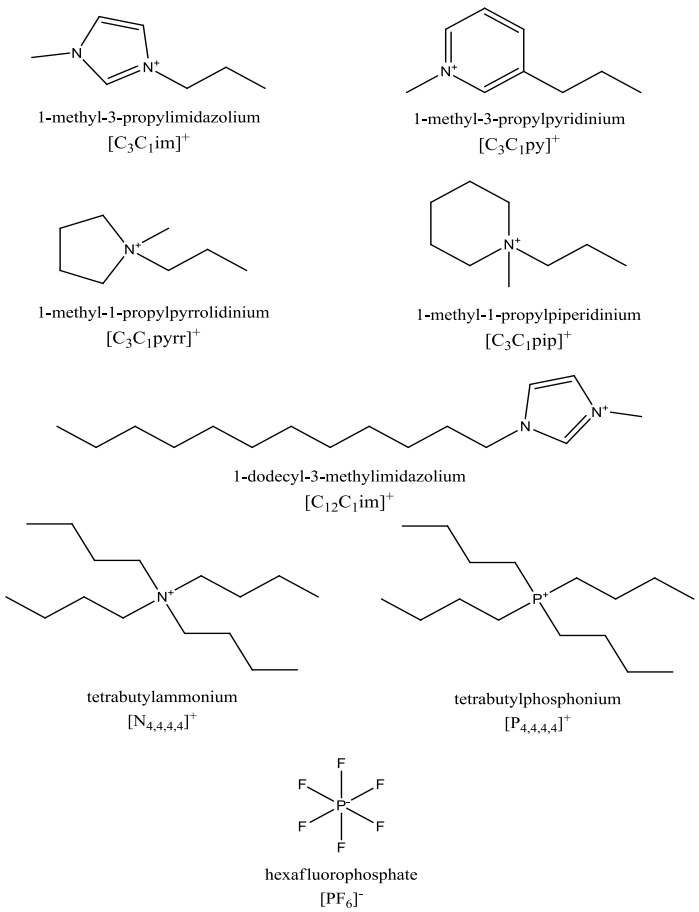

Figure 5 - Chemical structures of the cations and anions used for creating the binary mixtures of ionic liquids.

These ILs present mass fraction purities higher than 99%. The water content of all compounds was verified by Karl Fischer titration (Metrohm 831 Karl Fischer (KF) coulometer) and is presented in table 2. At least 3 measurements were conducted on the water content determination.

Table 2 – Name, supplier and water content of all the salts used in this work.

Sample	**Supplier**	**Purity / (wt %)**	**Water content (wt %)**
$[C_3C_1im][PF_6]$	IoLiTec	99.0	0.0104 ± 0.0017
$[C_3C_1py][PF_6]$	IoLiTec	99.0	0.2017 ± 0.0026
$[C_3C_1pip][PF_6]$	IoLiTec	99.0	0.0105 ± 0.0012
$[C_3C_1pyrr][PF_6]$	IoLiTec	99.0	0.0420 ± 0.0024
$[C_{12}C_1im][PF_6]$	IoLiTec	99.0	0.1044 ± 0.0007
$[N_{4,4,4,4}][PF_6]$	Appolo Scientific	98.0	0.1055 ± 0.0035
$[P_{4,4,4,4}][PF_6]$	Fluka	99.0	0.1228 ± 0.0016

2.1.1. **Preparation of mixture samples**

The binary mixtures were prepared by weighting ≈ 1 g of the mixture, composed of mole fractions of compound 1 comprised between x_1 = [0 to 1] with a estimated uncertainty of $\sigma_x = 5\times10^{-4}$ (in mole fraction), in an analytical balance (Mettler Toledo, Columbus, USA) with an uncertainty of ± 1×10^{-4} g. The binary mixtures, as depicted in figure 6, were heated to a temperature 10 K higher than the highest melting point of the two pure ionic liquids. Moreover, a continuous stirring under a nitrogen atmosphere, and until the mixture is completely melted was carried out, and then stayed for one hour at a constant temperature and under continuous stirring. After this step, the mixture was cooling down until room temperature at a temperature rate of circa to $5K{\cdot}min^{-1}$.

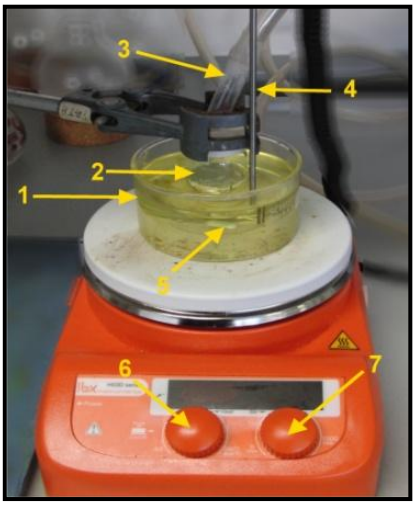

Figure 6 - Mixture mixing experimental scheme: 1- Vegetable oil bath; 2 – Sample vial; 3 – Nitrogen inlet to keep an inert atmosphere; 4 – Temperature sensor; 5 – Magnetic stirrer; 6 – Temperature controller; 7– Magnetic Stirrer rpm controller.

2.2. Experimental equipment and procedure

2.2.1. Differential Scanning Calorimetry

All the ionic liquids were submitted to differential scanning calorimetry (DSC) using a Q200 calorimeter (TA Instruments, New Castle, USA) for determining their melting temperature and melting enthalpy at ambient pressure. The DSC was previously calibrated with primary calibration standards, namely indium, naphthalene and cyclohexane, with weight fraction purities higher than 99.99%, and at a heating rate of 1 $K \cdot min^{-1}$. A constant flow of 50 $cm^3 \cdot min^{-1}$ of nitrogen was supplied to the DSC cell to avoid water condensation at lower temperatures. Approximately, 5 mg of each sample were sealed hermetically in aluminum pans and have been subjected to three heating and cooling cycles, between the temperatures ranging from 183.15 K to a temperature higher than the melting point in circa to 20 K, and at a constant cooling/heating rate of 1 $K \cdot min^{-1}$. The melting temperatures considered were the top peak values, and the temperature and enthalpy of melting were taken from the last heating run. The uncertainties of the melting temperatures and enthalpies were estimated according to the mean standard deviation of six replicates coupled to their standard deviations.

2.2.2. Temperature controlled polarizing optical microscopy

The binary mixtures melting temperatures were obtained by visual inspection of the salt melting using a temperature controlled polarizing optical microscopy (POM). For this purpose, as depicted in figure 7, an optical microscope Olympus BX-51 (Olympus Co., Tokyo, Japan) and an attached temperature controller stage, Linkam LTSE120 (Linkam Scientific Instruments Ltd., Tadworth, UK) with a precision of ± 0.05 K and with a limit temperature range between 248 K and 393 K, was used. A water pump ECP is coupled to the equipment to provide a temperature gradient to the peltier system when the stage is cooling or heating. The acquisition of images was carried out with a modified homemade apparatus, based on a webcam model Trust elight HD 1080P (Trust International B.V., Dordrecht, Netherlands) from which was taken a light filter, which allowed the CCD

sensor to receive the small amounts of light coming from the interior of the microscope. This procedure was adapted from telescope webcam technology.[96] This webcam is coupled to the microscope. Subsequently, the acquisition of images and videos was performed with a USB cable linked to the computer and with the use of a free software, namely MICAM© (Microscope Image Capture and Measurement) designed by Marien van Westen.[97]

The methodology used to accomplish the melting point data consisted in a first fast cooling and heating run with a temperature rate of 10 $K \cdot min^{-1}$ in order to evaluate the melting temperature range and if it was within the equipment limit. Then, after an isothermal treatment at 248.15 K for crystallization during 30 min, the samples were heated at 1 $K \cdot min^{-1}$ until reaching 10 K below the melting temperature, and then a rate of 0.1 $K \cdot min^{-1}$ was performed until all the sample was completely melted, this means, until the melting of the last small crystal observed on the microscope. The samples consisted in a small amount of mixture of approximately 5.0 mg, which were placed in a concave glass slide to maximize the contact between the liquid that starts forming and the melting solid mixture.

The evaluation of the accuracy of this equipment was performed by measuring melting points for some pure components and comparing them with data reported in literature[98] - table 3. Cyclohexane (99.9%, HPLC grade), octadecane (99%) all from Sigma-Aldrich (St. Louis, MO, USA), and tetradecane olefine free (99%) from Fluka (Buchs, Switzerland) were used. The absolute deviation (AD) was calculated by the absolute difference between experimental and literature data (equation 18). Observing the low absolute deviations it is possible to affirm that this technique is quite accurate.

$$AD = \left| T_{fus}^{exp} - T_{fus}^{literature} \right| \quad \textbf{(18)}$$

Table 3 – POM experimental measurements and DSC literature values for the melting points of some pure compounds.

Component	Our Work / (K)	Reference[98] / (K)	*AD* / **(K)**
Cyclohexane	279.45 ± 0.06	279.6 ± 0.3	0.15
Tetradecane	278.8 ± 0.06	278.7 ± 0.9	0.1
Octadecane	301.35 ± 0.06	301.0 ± 0.7	0.35

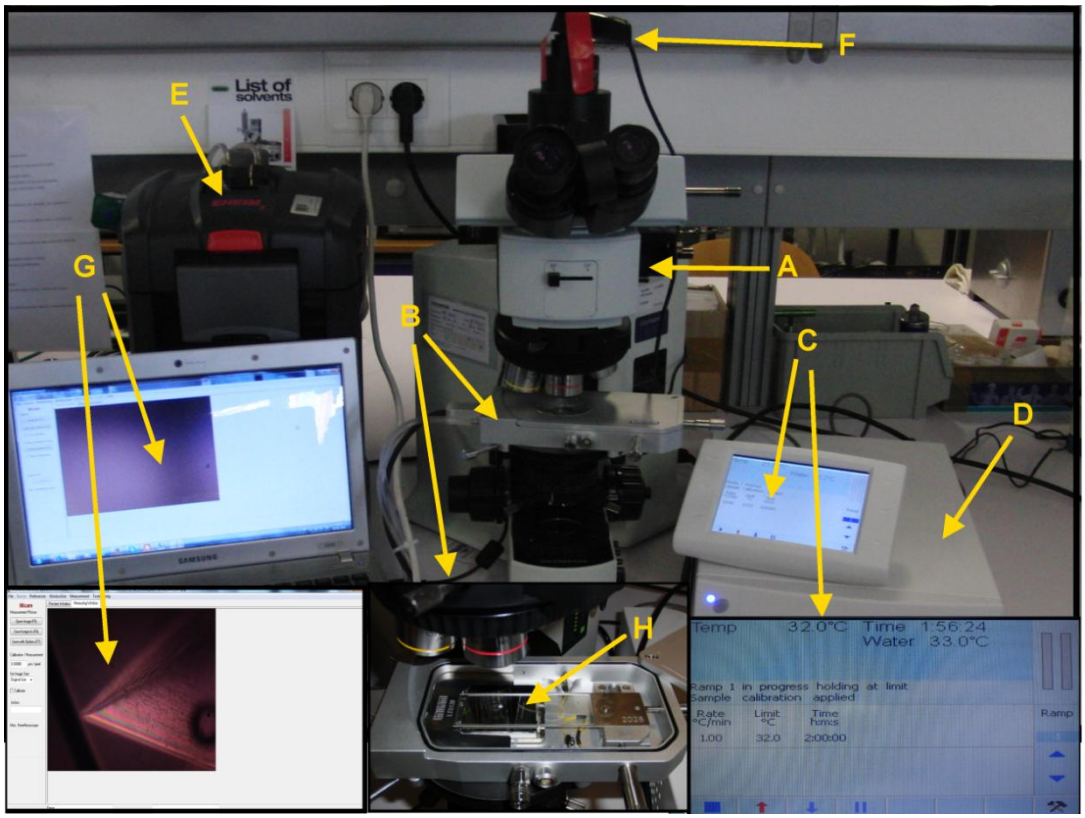

Figure 7 – Temperature controlled optical microscopy experimental scheme A - Olympus BX 51 optical microscope; B – Temperature controlled stage (Linkam LTSE 120); C – Controller with touch screen LCD for user interface (T95 LinkPad); D – Temperature controller device (T95-PE); E – Water pump for controlling the internal device temperature; F – Modified webcam for image and video acquisition (Trust Full HD Webcam); G – Computer with MICAM® software for image and video record; H – Concave slide glass.

2.2.3. Single crystal and Powder X-ray diffraction equipments

The pure compounds were investigated by single crystal X-ray diffraction at 180 K with monochromated Mo-K_α radiation (λ = 0.71073 Å) on a Bruker SMART Apex II diffractometer (Bruker, Billerica, USA) equipped with a CCD area detector. Data

reduction was carried out using a SAINT-NT software (Bruker, Billerica, USA) and multi-scan absorption corrections were applied to all raw intensity data using the SADABS program (Bruker, Billerica, USA). The structures were solved by a combination of direct methods with subsequent difference Fourier syntheses and refined by full matrix least squares on F^2 using the SHELX-97[99]. Anisotropic thermal parameters were used for all non-hydrogen atoms while the C-H hydrogen atoms were refined with isotropic parameters equivalent 1.2 times those of the atom to which they are bounded. Molecular diagrams were drawn with Mercury software (CCDC, Cambridge, UK).

For the powder X-ray diffractometry (XRD) it was used two different equipments. The XRD of the pure components $[C_3C_1pyrr][PF_6]$ and $[C_3C_1pip][PF_6]$ were performed with a Philips X'Pert - MPD diffractometer (Philips, The Netherlands). It was used monochromatic Cu-Kα radiation (λ=1.54180 Å) in the 3.50º- 49.98º 2Θ range and with a step of 0.04º(2Θ), at a rate of 35s *per* step. The measurements were made from 303 K to 390 and 376 K, respectively, for $[C_3C_1pyrr][PF_6]$ and $[C_3C_1pip][PF_6]$, with a heating rate of 1 $K \cdot min^{-1}$.

For the investigation of the system composed of $[C_3C_1pyrr][PF_6]$ and $[C_3C_1pip][PF_6]$, an Empyrean powder diffractometer (PANalytical, Almelo, Netherlands) was used. The measurements were made at room temperature (298 K), with nickel filter, Cu-Kα radiation (λ=1.54180 Å) step-scanned in 0.04º (2θ) at each 30 s, with a 2θ detection range from 4.01º to 49.98º.

3. Results and discussion

3.1. Solid-liquid phase behavior of pure ionic liquids

In order to accurately evaluate the solid-liquid equilibrium phase diagrams of the IL binary mixtures, it is crucial a fine understanding of the solid-liquid behavior of the respective pure components. Therefore, the melting enthalpies and temperatures for all the pure compounds used in this work were also determined by DSC in addition to POM. The melting temperatures and melting enthalpies and entropies of fusion of the pure ionic liquids are reported in table 4.

Based on the absolute value of the melting points it is possible to compare them, and to make some interpretations linking the melting points with the chemical structure of the compounds. Firstly, analyzing the increase on the alkyl side chain length in the imidazolium cation, $[C_3C_1im][PF_6]$ and $[C_{12}C_1im][PF_6]$, it is observed an increase in the melting temperature with the increase of the size of the aliphatic tail. This trend has already been reported previously by Lopez-Martinez *et al.*[100] which have seen a decrease from 403 K to 199 K, followed by an increase on the melting point from 199 K to 342 K, revealing thus a trendshift occurring at $[C_6C_1im][PF_6]$. A trend shift occurring for hexyl as the longest alkyl side chain in imidazolium-based compounds was also observed for other properties, such as densities, viscosities, refractive index (for the series of $[C_nC_1im][PF_6]$), volatility, enthalpy and entropy of vaporiztion (for the series of $[C_nC_1im][NTf_2]$).[101-103] Another parameter which one can evaluate using the available data is the effect of the aromaticity on the cation. It is clear that there is a difference between the compounds composed of an aromatic ring, *i.e.,* imidazolium and pyridinium, and which have lower melting temperatures comparing with those with a heterocyclic and saturated ring, respectively, the piperidinium and the pyrrolidinium-based ionic liquids. It is also possible to observe that the ILs composed of an aromatic ring do not present solid-solid transitions, contrarily to the others, that present two highly energetic solid-solid transitions of the same order of magnitude of the melting phase transition. Finally, the quaternary alkyl-based ionic liquids, $[N_{4,4,4,4}][PF_6]$ and $[P_{4,4,4,4}][PF_6]$, present higher melting points than the remaining compounds

investigated. The fact that these compounds exhibit a higher symmetry, than for example the alkylimidazolium-based compounds, allows us to probe the effect of the cation symmetry on the melting point that has been for long recognized.[63, 104] The melting temperature of the pure $[N_{4,4,4,4}][PF_6]$ and $[P_{4,4,4,4}][PF_6]$ were not measured by POM since the melting points of both compounds are higher than the maximum limit of the equipment, 393 K.

The uncertainty of the melting temperatures of the pure components obtained by microscopy was estimated to be not higher than σ_T = 1.30 K. This value was determined according to the mean values obtained by the evaluation of at least three replicates of the pure compounds. The mean absolute deviations between the two techniques were always lower than the uncertainty associated to the melting temperature obtained by the microscopy approach.

Table 4 - Melting and transition enthalpies, transition and melting temperatures and fusion entropies measured by DSC and melting temperatures obtained by POM, at a heating rate of 1K·min^{-1}.

IL	$[C_3C_1im][PF_6]$	$[C_{12}C_1im][PF_6]$	$[C_3C_1py][PF_6]$	$[C_3C_1pyrr][PF_6]$	$[C_3C_1pip][PF_6]$	$[N_{4,4,4,4}][PF_6]$	$[P_{4,4,4,4}][PF_6]$
POM - T_m (K)	311.1 ± 0.06	326.95 ± 0.15	311.6 ± 0.12	384.65 ± 0.06	370.65 ± 0.15	-	-
DSC Exp. T_m (K)	310.95 ± 0.04	326.30 ± 0.09	312.27 ± 0.27	382.45 ± 0.08	368.65 ± 0.09	524.3 ± 0.14	498.60 ± 0.03
DSC lit. T_m (K)	313.15[100]	328.15[100]		386.15[105]			
ΔH_{fusion} $(kJ \cdot mol^{-1})$	14.20 ± 0.08	25.82 ± 0.12	15.98 ± 0.19	3.39 ± 0.03	5.10 ± 0.01	16.41 ± 0.129	14.67 ± 0.02
T_{tr1} (K)	-	-	-	347.94 ± 2.22	312.37 ± 1.71	303.95 ± 0.26	263.63 ± 0.04
ΔH_{tr1} $(kJ \cdot mol^{-1})$	-	-	-	2.75 ± 0.09	8.07 ± 0.02	2.10 ± 0.04	1.81 ± 0.02
T_{tr2} (K)	-	-	-	359.57 ± 0.23	352.59 ± 0.02	360.70 ± 0.53	-
ΔH_{tr2} $(kJ \cdot mol^{-1})$	-	-	-	2.30 ± 0.02	5.10 ± 0.01	2.09 ± 0.53	-
ΔS_{fusion} $(J \cdot K^{-1} \cdot mol^{-1})$	49.78 ± 0.34	81.73 ± 1.32	44.56 ± 0.35	9.59 ± 0.15	14.37 ± 0.22	31.61 ± 0.55	29.75 ± 0.59

For some compounds showing solid-solid transitions, as revealed by the DSC experiments, it was also possible to confirm these transitions with crossed polarized light, and as shown in figure 8 for the $[C_3C_1pyrr][PF_6]$. In this example there are two highly energetic solid-solid transitions, presenting enthalpies of transitions comparable with the fusion enthalpy. For this compound it was possible to observe clear differences in the structure showing different polymorphic forms when comparing the figures 8a), 8b) and 8c). The refraction of the crystal, when observed by POM, undergoes several changes during the polymorphic transitions.

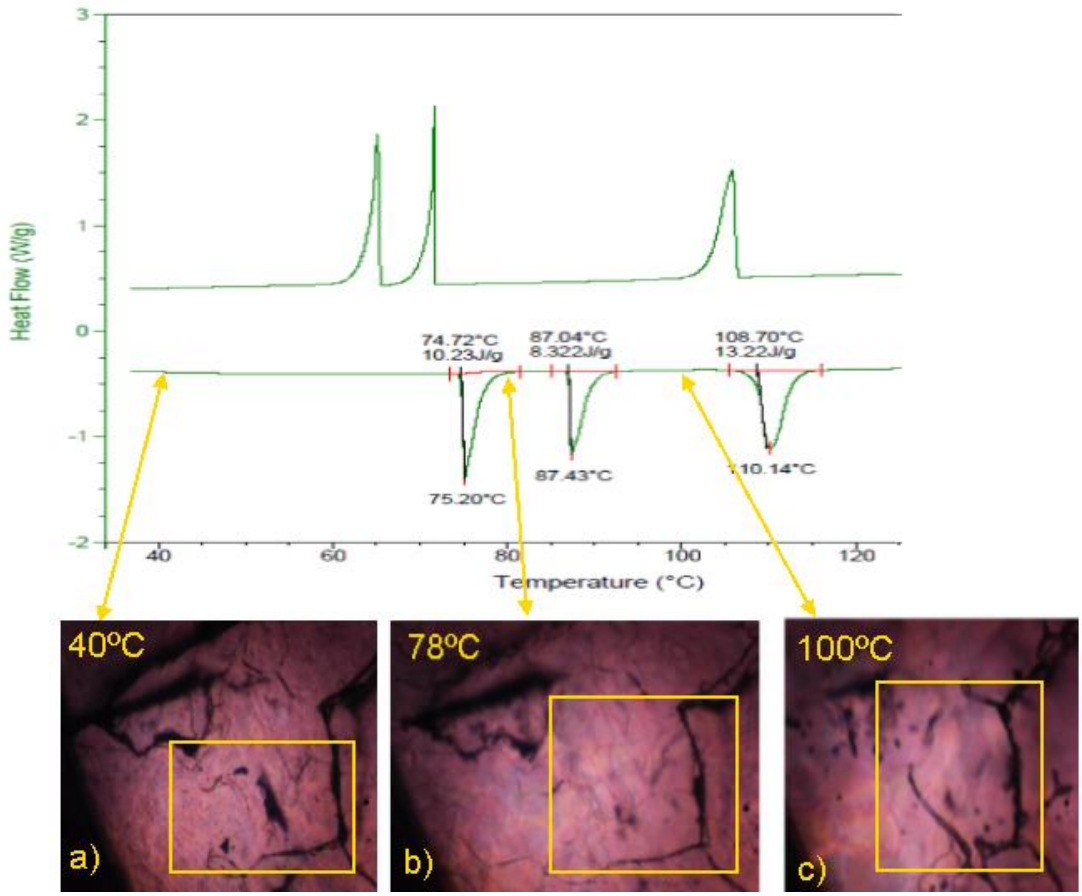

Figure 8 – DSC thermogram of pure 1-methyl-3-propylpyrrolidinium hexafluorophosphate and images acquired by POM at three different temperatures from the different polymorphic forms: a) $[C_3C_1pyrr][PF_6]$ at 313 K; b) $[C_3C_1pyrr]$ $[PF_6]$ at 351 K; c) $[C_3C_1pyrr]$ $[PF_6]$ at 373 K .

The diffractions patterns obtained by powder x-ray for the $[C_3C_1pyrr][PF_6]$ acquired for the same temperatures also corroborate the same idea. In figure 9, the disappearing of some intensity peaks and the appearance of new ones is presented for the different mesophases. The increase on temperature leads to a drastic reduction on the level of crystallinity of the salt, meaning that, although

being solid phases, a lower level of organization of the crystal lattice is presented for higher temperatures. The powder XRD also support the same pattern shifts for $[C_3C_1pip][PF_6]$ as one can see in appendix A.

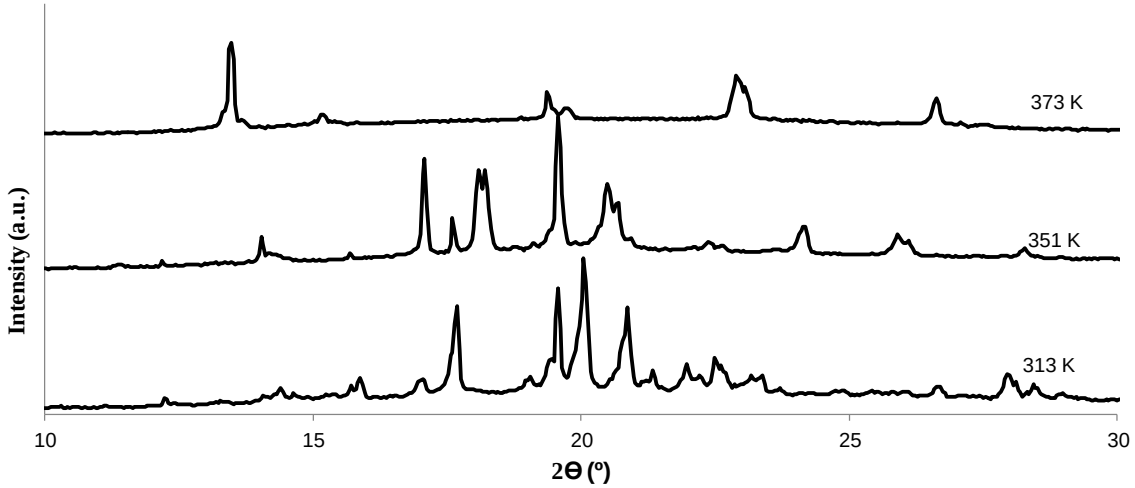

Figure 9 – Powder XRD patterns for pure $[C_3C_1pyrr][PF_6]$ at different temperatures, T = 313 K, T = 351 K and T= 373 K, illustrating the pattern shifts on the two S-S transitions.

One can suppose that high complex solid-solid transitions influence the melting temperature observed by POM, based on the last crystal melting and by this increasing the deviation from the DSC measurements. Even if the temperatures considered in this work by DSC measurements were the peak temperatures, contrarily to the most common onset temperatures, substantially higher deviations persist between POM and DSC for these compounds. One presume that the complexity of the solid phase leads to broad peaks in DSC measurements, representing less precision, contrarily to pure components that present much narrower peaks. Using the POM technique, it is possible to observe two distinct moments when reaching the melting temperature. The first, when almost all crystals melt, and that roughly corresponds to the melting temperature observed in the DSC measurements, and the last phase, an ionic plastic crystal phase. It could thus be assumed that the fusion enthalpy released by these metastable crystals is too low and can be considered negligible by DSC measurements, as suggested previously by Pringle *et al.*[106]. This introduces a greater difficulty on the observation and correct evaluation when considering the most accurate temperature for the melting point. This so-called plastic crystal phase behavior has

already been described by MacFarlane and co-workers[105], for the component [C_3C_1pyrr][PF_6]. Ohno *et al.*[107] reported the same behavior for a piperidinium hexafluorophosphate compound. One particular characteristic of these materials is a low fusion entropy, bellow 20 ($J{\cdot}K^{-1}{\cdot}mol^{-1}$), as the criterion established by Timmermans.[108] As can be observed in table 4 for the studied c,s [C_3C_1pyrr][PF_6] (9.59 ± 0.15 $J{\cdot}K^{-1}{\cdot}mol^{-1}$) and [$C_3C_1$pip][$PF_6$] (14.37 ± 0.22 $J{\cdot}K^{-1}{\cdot}mol^{-1}$), they obey this criterion. In the plastic crystal phase, ions have an enlarged degree of freedom, related to their isotropy and globular shape[108], allowing their rotational mobility, which can explain the increased conductivity on these phases.[109] Figure 10 shows a micrograph of one of these metastable crystals for [C_3C_1pyrr][PF_6].

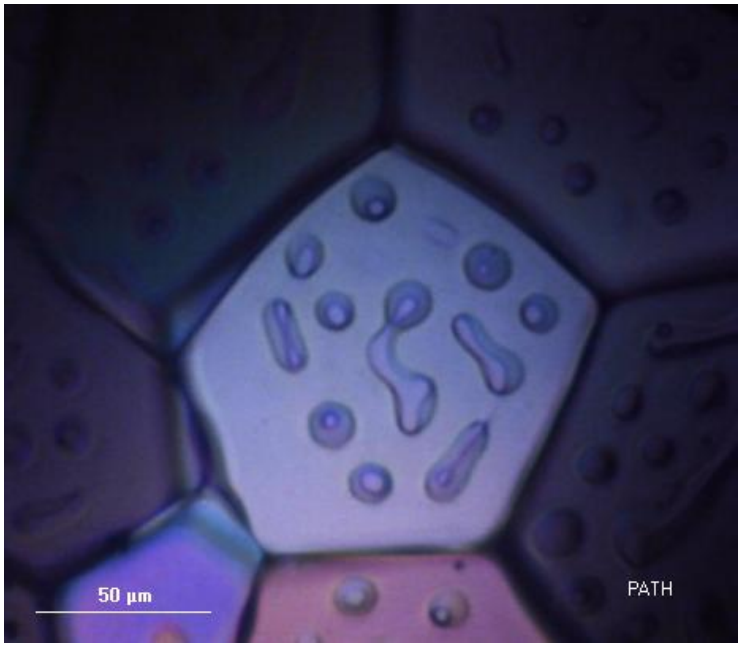

Figure 10 – Micrograph of the supposed plastic crystal of [C_3C_1pyrr][PF_6] before melting.

3.2. Crystallographic data of pure components

In order to better characterize the crystals of pure components, X-Ray acquisition was also performed. The unit cells for some components whose crystal data were obtained in this work are represented in figure 11. In the crystal packing of all compounds, non-covalent interactions are observed, including C–H···F hydrogen bonds with distances varying between 2.961(2) and 3.467(2) Å, which may play a role in the crystal lattice stabilization. The crystal structure results can provide relevant information to define the solid-liquid equilibrium thermodynamic profile of the mixtures as will be shown later. In table 5, all the crystal data obtained by X-ray are reported.

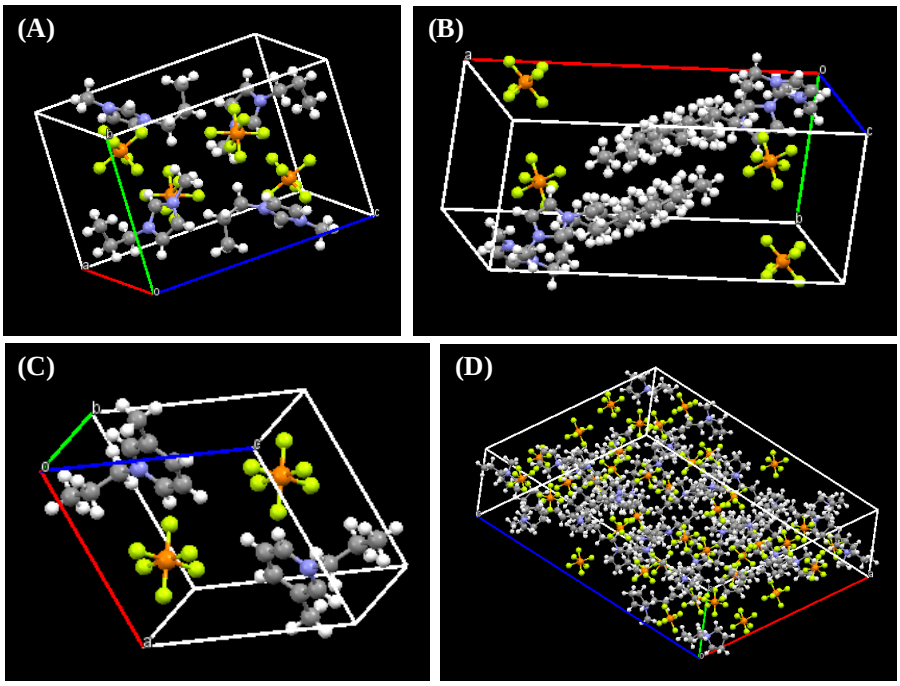

Figure 11 - Molecular diagrams showing the unit cell of pure (A) [C_3C_1im][PF_6], (B) [$C_{12}C_1$im][PF_6], (C) [C_3C_1py][PF_6] and (D) [C_3C_1pyrr][PF_6] (CCDC code: QOPZUQ), drawn with Mercury 3.1 software (CCDC, Cambridge, UK) (download available in http://www.ccdc.cam.ac.uk/mercury). Color scheme: C, grey; N, blue; O, red; H, white; P, orange; and F, green.

Table 5 - Crystal data and selected refinement details for the compounds $[C_3C_1im][PF_6]$, $[C_{12}C_1im][PF_6]$, $[C_3C_1py][PF_6]$, $[C_3C_1pyrr][PF_6]$ and $[C_3C_1pip][PF_6]$.

Compound	$[C_3C_1im][PF_6]$	$[C_{12}C_1im][PF_6]$ [f]	$[C_3C_1py][PF_6]$	$[C_3C_1pyrr][PF_6]$ [¥]	$[C_3C_1pip][PF_6]$
Formula	$C_7H_{13}F_6N_2P$	$C_{16}H_{31}F_6N_2P$	$C_9H_{14}F_6NP$	$C_8H_{18}F_6NP$	$C_9H_{20}F_6NP$
M_w ($g \cdot mol^{-1}$)	270.16	396.40	281.18	273.20	287.23
Crystal System	Monoclinic	Monoclinic	Triclinic	Monoclinic	Monoclinic
Space group	*P 2₁/c*	P *2₁*/c	*P -1*	*C 2/c*	*P 2₁/c*
a (Å)	8.5236(14)	22.2422(8)	8.8517(5)	25.0964(7)	14.4143(7)
b (Å)	10.0435(17)	9.8387(3)	9.1524(5)	13.5788(5)	14.2106(8)
c (Å)	13.640(3)	9.2465(3)	9.2668(5)	34.0634(13)	13.4918(6)
α (°)	(90)	(90)	63.953(5)	(90)	(90)
β (°)	106.075(5)	94.611(2)	64.555(2)	109.797(1)	109.466(2)
γ (°)	(90)	(90)	85.076(2)	(90)	(90)
V ($Å^3$)	1122.0(3)	2016.90(12)	604.15(6)	10922(4)	2605.6(2)
Z (Z')	4	4	2	36	8
D_c ($Mg \cdot m^{-3}$)	1.599	1.305	1.546	1.495	1.464
μ (mm^{-1})	0.302	0.191	0.282	0.277	0.262
reflections collected	27615	21166	22246	33739	1907
unique reflections, [R_{int}]	4326, [0.0243]	4137, [0.0355]	4662, [0.0206]	10190, [0.048]	7003, [0.0654]
Final *R* indices					
R_1, wR_2, [I>2σI]	0.0468, 0.1275, [3583]	0.0424, 0.1035, [3001]	0.0443, 0.1227, [3940]	0.0775, 0.1985 [6622]	0.0554, 0.1297 [4055]
R_1, wR_2 (all data)	0.0565, 0.1364	0.0654, 0.1158	0.0522, 0.1314	0.1241, 0.2320	0.1118, 0.1586

[f] Crystal structure parameters obtained in this work, comparable to those published by Gordon *et al.*[73]. [¥] Crystal data from literature[105] at 123 K.

3.3. Evaluation of the mixtures' experimental solid-liquid equilibrium behavior

In this work nine binary systems were prepared composed of components with the most commonly used cations and with a fixed anion, hexafluorophosphate, as shown in table 6. The binary mixtures composed of $[C_3C_1im][PF_6]$ + $[N_{4,4,4,4}][PF_6]$ and $[C_3C_1im][PF_6]$ + $[P_{4,4,4,4}][PF_6]$ were only partially studied, for a mole fraction of $[C_3C_1im][PF_6]$ higher than 0.7, since for mole fractions richer in the tetraalkyl-based compounds have melting temperatures higher than 393.15 K, being this the upper limit of temperature of the POM equipment. This is a major limitation on the complete description of these two systems.

Table 6 - Matrix containing all the studied binary mixtures composed of the several cations and the common $[PF_6]^-$ anion: ◆ , Binary mixture studied; ◇ , Binary mixture not studied.

$[PF_6]^-$	$[C_{12}C_1im]^+$	$[C_3C_1py]^+$	$[C_3C_1pyrr]^+$	$[C_3C_1pip]^+$	$[N_{4,4,4,4}]^+$	$[P_{4,4,4,4}]^+$
$[C_3C_1im]^+$	◆	◆	◆	◆	◆	◆
$[C_3C_1py]^+$	◇	◆	◆	◆	◇	◇
$[C_3C_1pyrr]^+$	◇	◇	◆	◇	◇	◇

From this point, the solid-liquid phase diagrams determined by POM for all the binary mixtures, with the exception of the system composed of $[C_3C_1pyrr][PF_6]$ + $[C_3C_1pip][PF_6]$, are presented in figure 12. Later, this system will be presented in detail because of the particular characteristics on the solid-liquid phase behavior of this mixture.

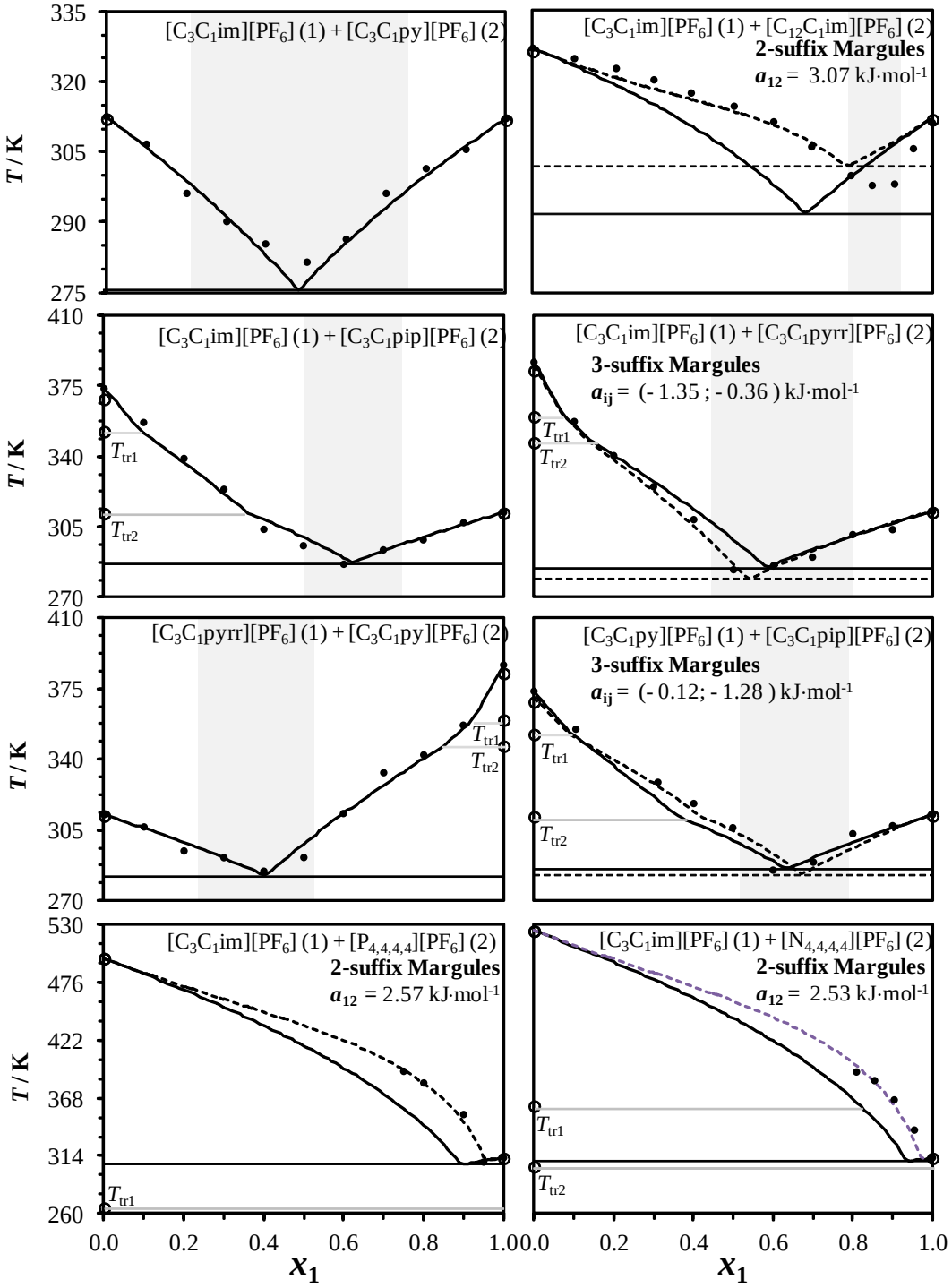

Figure 12 – Solid-liquid phase diagrams (temperature, T / K, *versus* mole fraction of the component 1, x_1) of the mixtures studied. Melting temperatures obtained by optical microscopy (●); melting and solid-solid transitions temperatures obtained by DSC (○); modeling results considering $\gamma_i^L = 1.0$ and $x_i^S\gamma_i^S = 1.0$ (full lines), and using 2 or 3-suffix Margules (dashed lines). Grey lines represent the solid-solid transitions temperatures, T_{tr1} and T_{tr2} (from table 4). Grey regions highlight the concentration range for which the mixture is liquid at room temperature (T = 298.15 K).

All the SLE phase diagrams studied exhibit an eutectic-like phase behavior. These eutectic-like behaviors can lead to new ionic liquids since a major depression on the melting point corresponding to the eutectic composition can be reached. These results show that it is possible to depart from two compounds with melting points higher than room-temperature, and just by mixing them, reaching a component presenting a lower melting temperature, and in most cases lower than room-temperature. In fact, it is possible to observe massive melting temperature depressions, where in some examples the difference between the melting temperature of the pure and the eutectic composition can reach 100 K. The higher melting depression is observed in the system composed of $[C_3C_1im][PF_6]$ + $[C_3C_1pyrr][PF_6]$, where the temperature depression between the pure melting temperature of $[C_3C_1pyrr][PF_6]$ (384.65 K) and the melting temperature on the eutectic composition (x_1 = 0.501; T = 283.15 K) reaches 101.5 K.

The eutectic temperatures, with the exception of the ammonium- and the phosphonium-based salts mixtures with $[C_3C_1im][PF_6]$, are all below or close to room-temperature, *i.e*, 298.15 K. This is affected by the melting temperature of the pure component, as in the mixtures composed of the tetrabutylammonium and phosphonium cations, the pure components present a high melting temperature, and then, the depression on the melting point is not enough to reach a temperature at or below room temperature. The range of compositions at which the melting temperatures are below room-temperature is dependent on the mixture under study, and as seen in figure 12, where the grey zones represent the *liquidus* range at room-temperature. For instance, the SLE phase diagram of the mixture composed of $[C_3C_1im][PF_6]$ and $[C_3C_1py][PF_6]$, presents a broader range of composition at which the melting temperature is at or below room-temperature, when compared, for example, with a narrower *liquidus* range in the system $[C_3C_1im][C_{12}C_1im][PF_6]$. These results show that one of the main goals of this work, to generate new materials exhibiting a larger *liquidus* range through the understanding of the solid-liquid phase behavior of mixtures composed of ionic solids, was attainable. The lowering of the melting points of mixtures confers to these new materials the possibility of enlarging their range of applications in chemical engineering processes.

3.4. Modeling the solid-liquid phase behavior

The first approach to describe the solid-liquid phase behavior, as written previously, consisted on a simpler thermodynamic approach considering an ideal behavior of the liquid and pure solid phases.

On a first glance at the experimental phase behavior obtained by POM, it is evident that in most systems an ideal behavior is followed. Most experimental data for the melting temperatures for the different compositions of the different systems can be well-described by the *liquidus* line calculated by equation 8. As described previously, it is assumed the liquid ideal behavior, considering the activity coefficient, γ_i^L, equal to one, and the immiscibility of the solid phase. Furthermore, the heat capacity factor was neglected.

A point that further evaluated was the introduction on this analysis of the contribution of the solid-solid transitions. In literature[82, 85], the contribution of this term for the modeling of the phase behavior is often considered as negligible. The reason for this is that, commonly, these transitions present much lower enthalpies when comparable with fusion enthalpies. Furthermore, the transition temperatures may be too far from the melting temperature, thus presenting no effect on the eutectic point, or too close to the melting temperature, and can thus be considered as part of the melting process. This has guided us to be cautious on the assessment of the effect of the solid-solid transitions enthalpies and temperatures of the components. As discussed previously, most of our components present high absolute values of solid-solid transition enthalpies, too high to not being considered into the modeling. Moreover, the transition temperatures are too different from the melting temperatures to be considered as a part of the melting process, but close enough so that they are above the eutectic temperatures and therefore must be taken into account. An example of this effect is depicted in figure 13, for the system composed of $[C_3C_1im][PF_6]$ and $[C_3C_1pip][PF_6]$, where one can observe the difference between the modeling considering the term related with the polymorph transitions for $[C_3C_1pip][PF_6]$ and neglecting them. Taking the solid-solid transitions into account a near-ideal behavior is observed.

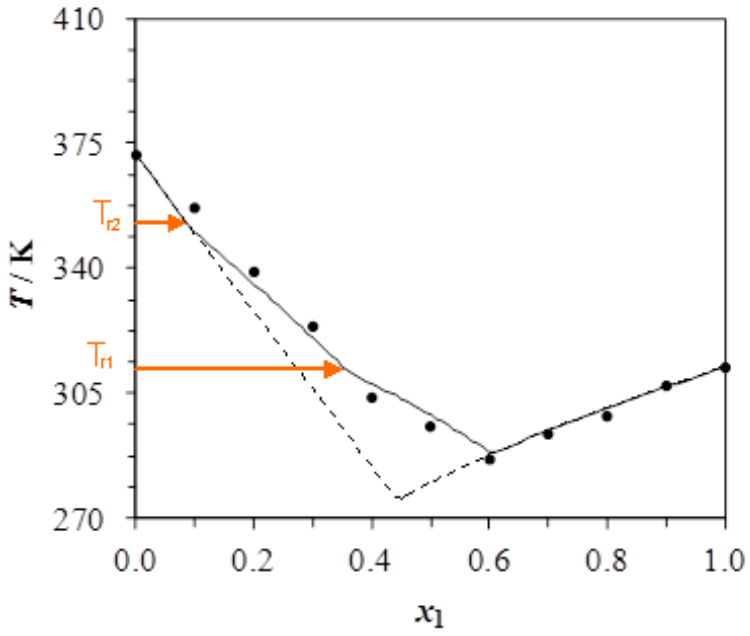

Figure 13 - Comparison between the modeling of the SLE ideal phase behavior diagram, considering the ideal assumptions model (γ_i^L = 1.0, $x_i^S \gamma_i^S$ = 1.0), for the mixture composed of [C_3C_1im][PF_6] and [C_3C_1pip][PF_6], introducing the polymorph transition term (dashed line) or neglecting it (solid line) into the calculations of the ideal model, and comparing them with the experimental data obtained by POM (•).

The fact that the studied systems behave approximately as ideal, exhibiting an eutectic behavior, means that they can be well and easily predicted by an ideal model without adjustments on the non-ideal parameter, the liquid phase activity coefficient (γ_i^L). The solid-liquid phase behavior can be estimated from the knowledge of the melting enthalpies and temperatures, as well as the solid-solid transitions of the pure compounds that compose the binary mixtures.

3.5. Non-ideal behavior assessment on IL-IL mixtures

Figure 12 reports the activity coefficients estimated for all the systems studied using equation (9). It is shown that only three binary mixtures, [C_3C_1im][C_3C_1py][PF_6], [C_3C_1im][C_3C_1pip][PF_6] and [C_3C_1pyrr][C_3C_1py][PF_6], can be rigorously considered as ideal. In the other systems, slight positive and negative deviations are observed. This is the case of the mixtures composed of [C_3C_1im][C_3C_1pyrr][PF_6] and [C_3C_1py][C_3C_1pip][PF_6]. In the case of

$[C_3C_1im][C_3C_1pyrr][PF_6]$, minor negative deviations are observed in the domains of both component mole fractions. Contrarily, the $[C_3C_1py][C_3C_1pip][PF_6]$ binary mixture exhibits positive deviations only observed in the piperidinium-rich region. In the pyridinium-rich phase the mixture behaves ideally. These deviations occur mostly around the eutectic region. In these two examples, an insightful evaluation of all the parameters leads us to assume that the mixtures behave as ideal or almost ideal. The assumptions made to calculate the ideal model, as for example while neglecting the heat capacities, and also the uncertainty associated to the method and experimental procedure, are sufficient to cover the differences between experimental data and ideal behavior.

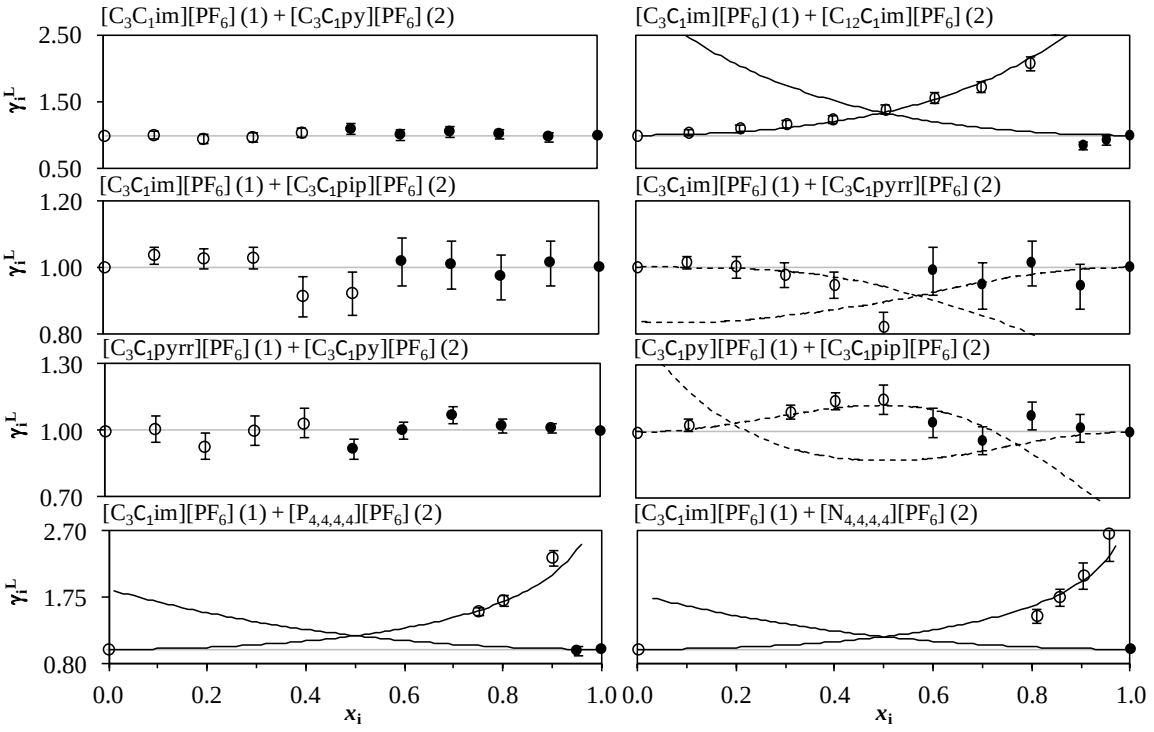

Figure 14 - Liquid phase's activity coefficients of component 1 (•) and 2 (○) calculated by Eq. (3) and using γ_i^L equations: 2-suffix-Margules (full lines) and 3-suffix-Margules (dashed lines). Error bars were calculated by error propagation at the 0.95 confidence level.

In the remaining cases, the binary mixtures composed of $[C_3C_1im][PF_6]$ with $[C_{12}C_1im][PF_6]$, $[N_{4,4,4,4}][PF_6]$ and $[P_{4,4,4,4}][PF_6]$, the liquid phase non-ideal behavior is more significant. This is as expectable trend if an inspection of the molecular structure of the components is carried out. The systems described above present a high similarity between the cations, simply differing in the ring size, such as

pyridinium and imidazolium which differ only in one carbon atom, or differing in the aromatic character as the pyrrolidinium and imidazolium or piperidinium and pyridinium, which leads them to generate ideal liquid mixtures. Here, the mixing of components significantly different in terms of the cation molecular structure opens the path to a non-ideal behavior of the mixtures.

In the case of the mixture composed of $[C_3C_1im][PF_6]$ and $[C_{12}C_1im][PF_6]$, a patent positive deviation is observed in the region rich in $[C_{12}C_1im][PF_6]$ reaching activity coefficients higher than two, while in the narrow domain of $[C_3C_1im][PF_6]$, slight negative deviations are observed. One could expect that the entropic effect of the introduction of a component with a shorter alkyl chain would generate a negative deviation, but precisely the opposite is happening. A high positive deviation to ideality is observed. This can be explained as a result of the highly ordered nanostructure, an interdigitated ion-ion nanostructure[73, 110], as seen in figure 15, which can result into stronger and more favorable interactions between the ions of $[C_{12}C_1im][PF_6]$.

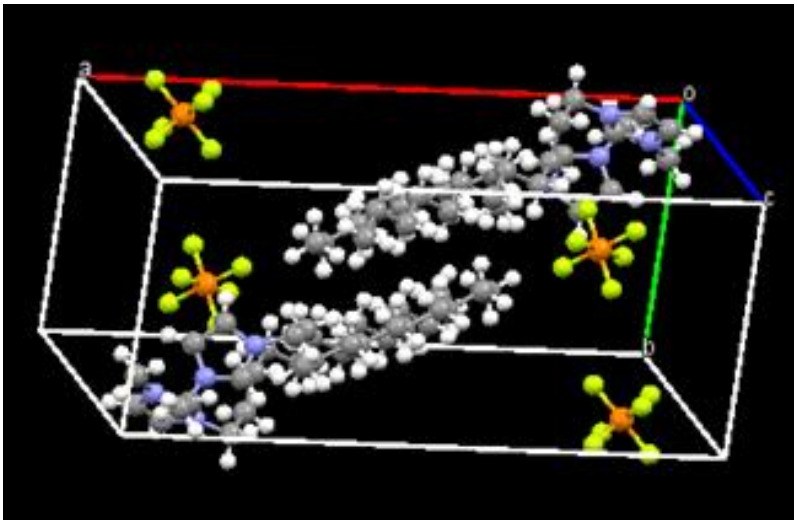

Figure 15 - Molecular diagram showing the unit cell of pure $[C_{12}C_1im][PF_6]$. (CCDC code: QOPZUQ), drawn with Mercury 3.1 software (CCDC, Cambridge, UK) (download available in http://www.ccdc.cam.ac.uk/mercury). Colour scheme: C, grey; N, blue; O, red; H, white; P, orange; and F, green.

For the mixtures composed of $[C_3C_1im][PF_6]$ and $[N_{4,4,4,4}]$ $[PF_6]$ or $[P_{4,4,4,4}][PF_6]$, although only restricted parts of the phase diagrams were measured due to

limitations on the experimental technique used, high deviations from the ideal behavior were observed. In these two examples the differences between the molecular cation structures are evident and the deviations to the ideal behavior are thus expectable. From one side, the $[C_3C_1im]^+$ cation, containing an aromatic ring and presenting an evident asymmetry, whereas on the other side, two aliphatic tetraalkyl cations are present with marked symmetry. However, the evaluation on the general phase behavior is possible despite some limitations on the phase diagram. The first inference that can be made is that the eutectic region on these systems is too close to the $[C_3C_1im][PF_6]$ pure concentrations meaning that the information on the imidazolium-rich region is too short to allow conclusions about the deviations of ideality on this side of the phase diagram. In addition, the limitation imposed by the equipment to make measurements in the region of high concentrations of tetraalkylammonium or phosphonium cations, since they present melting temperatures over the 393 K, is a major drawback. Even so, one can presume that the interactions between the tetraalkyl cations with similar cations are much stronger than the interactions between unlike cations, *i.e*, tetraalkyl and 1-propyl-3-methylimidazolium cations. This leads obviously to a non-ideality displayed by these two mixtures.

In order to describe the non-ideal liquid phase behavior, it was used the 2- or 3-suffix Margules model[82, 85] (equations 10 and 11) for the calculations of the liquid phase activity coefficients, γ_i^L. Based on these activity coefficients it was possible to calculate the non-ideal phase behavior profiles. As seen in figure 12, in the dashed lines, they describe well the non-ideal phase behavior in the whole solid-liquid phase diagram except in the case of the system composed of $[C_3C_1im][PF_6]$ and $[C_{12}C_1im][PF_6]$. In this example, deviations of opposite type do not allow the modeling description of the eutectic behavior.

3.6. **COSMO-RS**

In this work, it was evaluated the ability of COSMO-RS to predict the phase behavior of the studied systems by comparing it with the experimental data. In order to evaluate the accuracy of the model to describe the non-ideality, the activity coefficients were calculated for the eight previously studied eutectic

systems. Thenceforth, they were compared with the experimental data, as reported in figure 16. It was found that COSMO-RS is able to forecast accurately the deviations from ideal behavior. In fact, the systems that presented higher deviations to ideality, the mixtures composed of quaternary alkyl-based ionic liquids, $[N_{4,4,4,4}][PF_6]$ and $[P_{4,4,4,4}][PF_6]$ and $[C_3C_1im][PF_6]$, and also the mixture composed of $[C_3C_1im][PF_6]$ and $[C_{12}C_1im][PF_6]$, are well described by COSMO-RS. For the systems that present minor deviations, as for example for the mixture composed of $[C_3C_1py][PF_6]$ and $[C_3C_1pip][PF_6]$ that presents slight deviations, COSMO-RS can't describe these small deviations from ideal behavior.

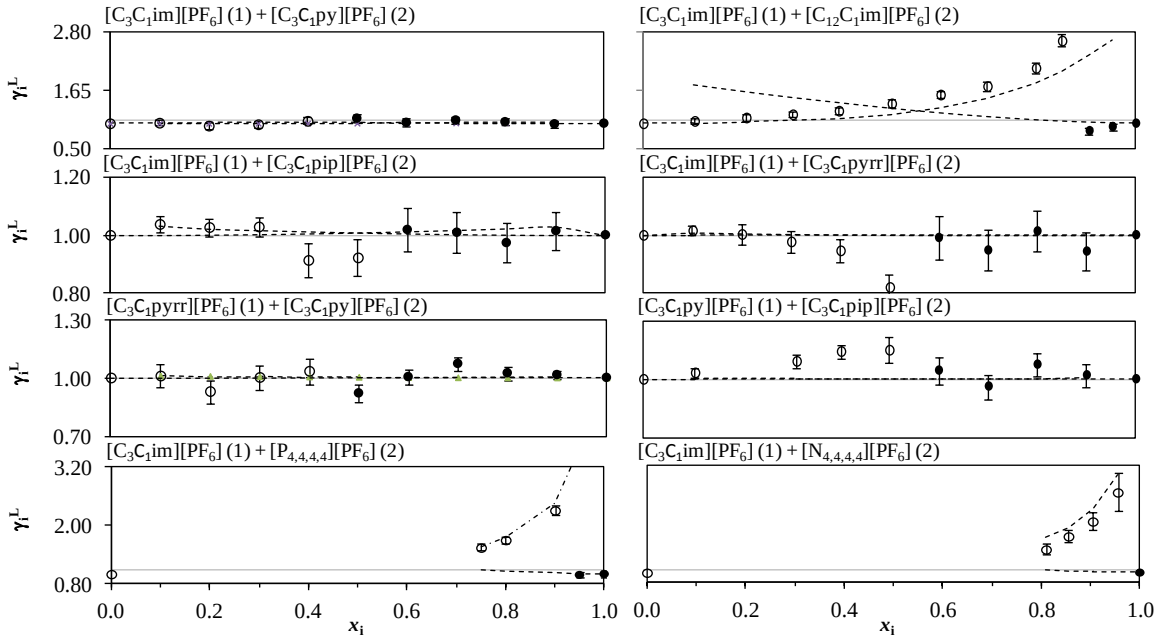

Figure 16 - Liquid phase's activity coefficients of component 1 (•) and 2 (○) calculated by Eq. (3) and γ_i^L predicted by COSMO-RS model (dashed lines). Error bars were calculated by error propagation at the 0.95 confidence level.

For the systems where higher deviations from ideality are observed, and for which COSMO-RS can predict these deviations, as for the quaternary alkyl-based ILs, the contributions for these deviations were evaluated in terms of the excess enthalpies not only for the total, but also for the electrostatic, hydrogen-bonding and van der Waals interactions. The individual contributions of each ion are presented in appendix C. In both cases, the quaternary alkyl cations are predicted as the main responsible to the positive deviations to ideality observed, presenting higher positive values for the excess enthalpies. This indicate that these cations

interact preferably with similar than with unlike ions in the mixture, which corroborates what was stated previously and the expectable trend. The misfit interactions are predicted as the main contributors for the global positive deviations since higher excess enthalpies values, corresponding to this kind of interactions, are observed when compared with excess enthalpies corresponding to hydrogen-bonding or van der Waals interactions.

The COSMO-therm software permits to forecast SLE phase diagrams of IL-IL mixtures, only based on the melting point and fusion enthalpy of the pure components that compose the mixture, as in the examples presented in the phase diagrams of the eutectic systems composed of $[C_3C_1im][C_3C_1py][PF_6]$ and $[C_3C_1im][C_{12}C_1im][PF_6]$. Nevertheless, it was also observed that since it is not possible to introduce the solid-solid transitions enthalpies and temperatures into COSMO-RS calculations, these contributions are neglected when predicting the phase diagrams. This leads to higher deviations between the calculated and the experimental data in the systems composed of ionic liquids presenting higher solid-solid transitions and temperatures close to solid-liquid transition.

Summarizing, in this work it is shown that COSMO-RS can be used as a predictive tool for describing the IL-IL mixtures SLE phase behavior. This model also leads to valuable information towards the understanding on the main important interactions occurring between the components in the mixtures and which majorly contribute to the non-ideality.

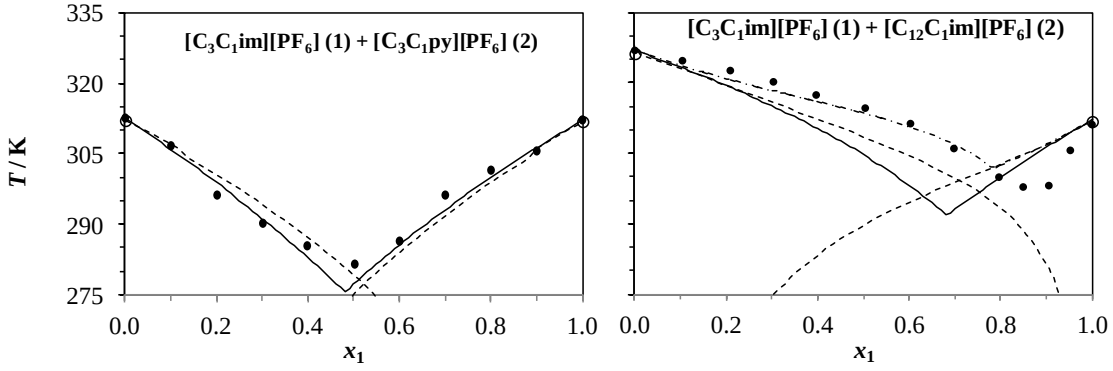

Figure 17 - Comparison between the modeling of the SLE ideal phase behavior diagram, considering the ideal assumptions model (γ_i^L = 1.0, $x_i^S\gamma_i^S$ = 1.0) (solid lines), the COSMO-RS predicted phase behavior diagrams (dashed line), from the mixtures composed of $[C_3C_1im][PF_6]$[C_3C_1py][PF_6] and $[C_3C_1im][PF_6]$[$C_{12}C_1im$][PF_6], and comparing them with the experimental data obtained by POM (•). In the case of $[C_3C_1im][PF_6]$[$C_{12}C_1im$][PF_6] it is also compared the modeling with 2-suffix Margules (dotted and dashed line).

3.7. The exceptional behavior of the mixture composed of $[C_3C_1pyrr][PF_6]$ and $[C_3C_1pip][PF_6]$: the formation of an alloy

As previously mentioned, the mixture composed of $[C_3C_1pyrr][PF_6]$ and $[C_3C_1pip][PF_6]$ exhibits a unique behavior, unlike any other of the systems studied. This mixture exhibits a very uncommon non-eutectic phase behavior contrarily to all the other systems presented before. In order to evaluate this behavior, additionally to POM, two other techniques were employed, namely the DSC at all the compositions and powder X-ray diffractometry of the solid phase. These two techniques allow us to corroborate the results obtained by POM.

The thermograms obtained by DSC, reported in figure 18, present only an endothermic peak on the melting process, contrarily to what is observed for most of the mixtures that exhibit two endothermic peaks, one related with the eutectic transition and another at the melting temperature.[1, 111-112] Moreover, this behavior is in agreement with that observed by POM. This led us to believe that the mixture forms a continuous solid solution and thus forms an alloy.

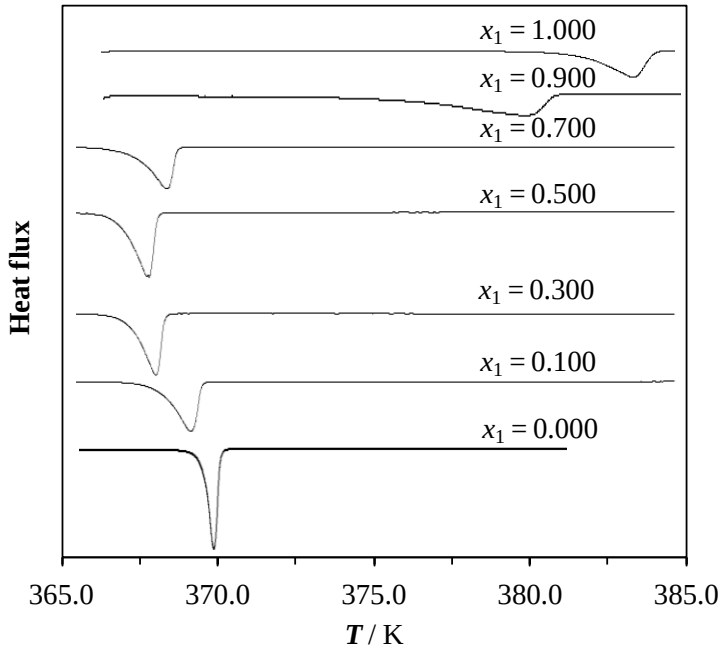

Figure 18 – Thermograms obtained by DSC regarding the phase behavior of the binary mixture composed of $[C_3C_1pyrr][PF_6]$ and $[C_3C_1pip][PF_6]$.

In a solid state, the solid phase exhibits a monophasic region and both components crystallize on a single crystal lattice. In order to prove this behavior of our mixture, powder X-ray diffractometry of the solid phase was performed. This experiment revealed that the patterns change rapidly, just after $x_1 = 0.05$, and from those of pure $[C_3C_1pip][PF_6]$ for those of pure $[C_3C_1pyrr][PF_6]$ as seen in figure 19, and that this pattern is maintained in all the entire range of composition. This behavior is different from what is expected when the mixtures display immiscibility in the solid region. In this case, the diffractograms would display the diffraction peaks from both pure components. The diffractograms reported in figure 19 confirm that a monophasic alloy is formed in this system.

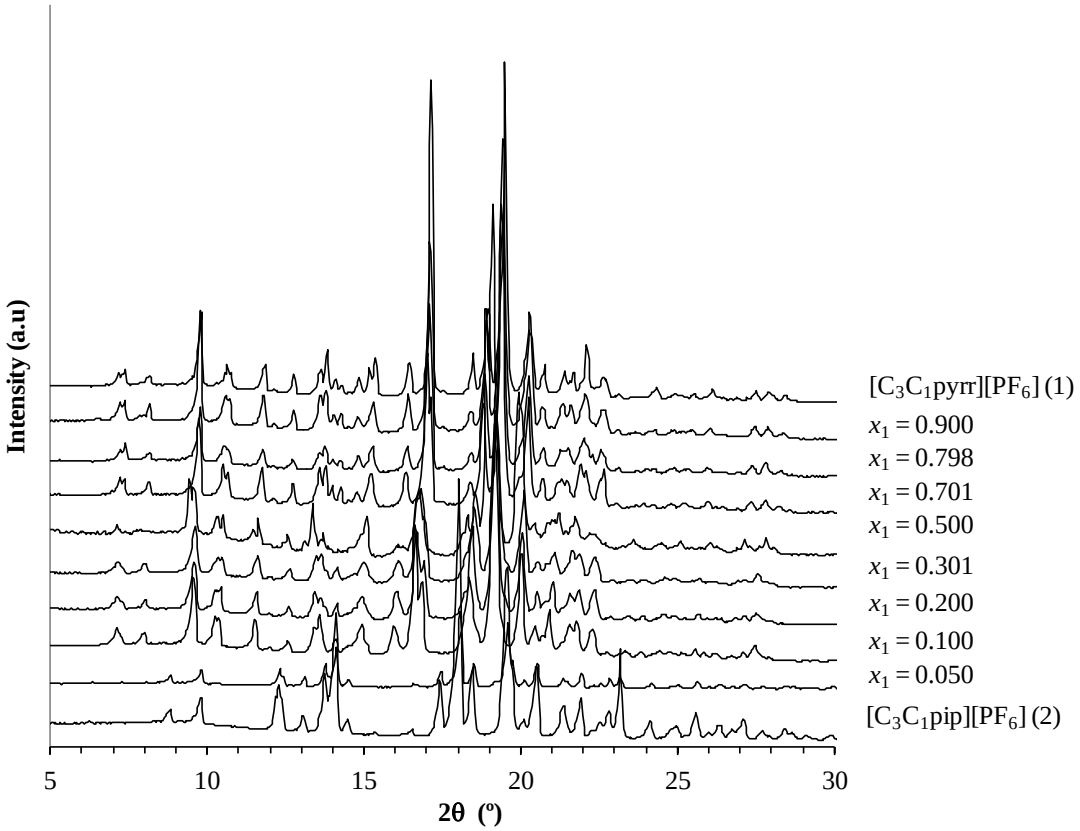

Figure 19 - Powder XRD patterns of the $[C_3C_1pyrr][PF_6]$ (1) and $[C_3C_1pip][PF_6]$ (2) mixture at T = 298.15 K.

The similarities of the crystallographic structures of the two pure compounds leads us to assume that the $[C_3C_1pip][PF_6]$ crystal is incorporated as a guest in the crystalline lattice of $[C_3C_1pyrr][PF_6]$. Moreover, the single crystal X-ray data, presented in table 5, concedes additional information in order to understand this behavior. It can be observed that the two components are very similar since they present a monoclinic unit cell containing exactly the same crystallographic axes. In addition, for the crystal packaging there are some substantial differences since $[C_3C_1pip][PF_6]$ presents only eight unit cells while $[C_3C_1pyrr][PF_6]$ presents 36. Since the volumes of the crystalline structure are quite different, this can reveal the ability of the $[C_3C_1pyrr][PF_6]$ to act as host-structure to $[C_3C_1pip][PF_6]$, and by this, allowing the $[C_3C_1pip][PF_6]$ crystal to accommodate into its structure. This behavior was also reported by Gordon *et al.*[73], when studying the solid-liquid equilibrium of a mixture composed of $[C_{16}C_1im][PF_6]$ and $[C_{16}py][PF_6]$ in order to obtain an eutectic mixture. In this case, a continuous solid-solution is also displayed but

containing long alkyl chain length cations, contrarily to our components that have short alkyl chains.

In figure 20 it is possible to observe the comparison between the experimental melting temperatures observed by POM and DSC. It is also depicted the ideal behavior profile and the modeling of the non-ideal behavior. One should note that the observations done by POM, were affected by the formation of some metastable crystals, supposedly plastic crystals, while the melting was occurring, and which adds a major difficulty to the observation and identification of the last melting crystal.

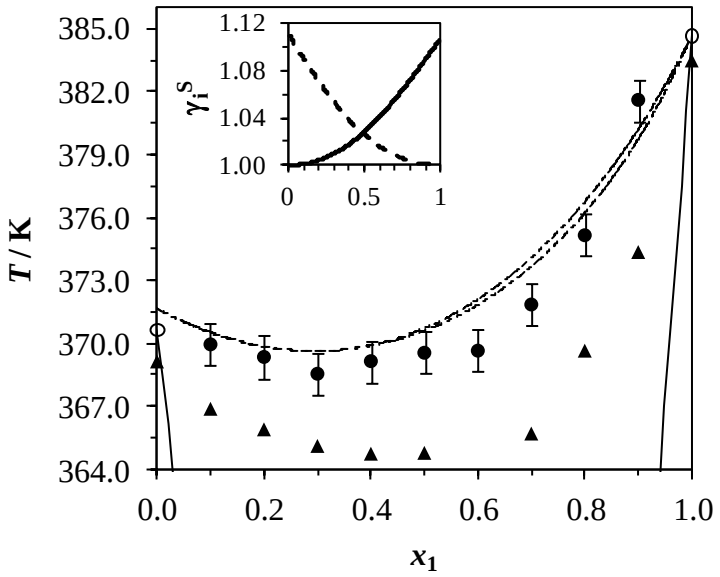

Figure 20 – Solid-liquid equilibrium phase diagram of the $[C_3C_1pyrr][PF_6]$ (1) and $[C_3C_1pip][PF_6]$ (2) mixture with experimental data obtained by POM (•) or by DSC (▲). Model results considering $\gamma_i^L = 1.0$ and $x_i^S\gamma_i^S = 1.0$ (dashed lines), and considering $\gamma_i^L = 1.0$ and $\gamma_i^S \neq 1.0$ using 2-suffix-Margules equation (solid lines) with binary interaction parameter $a_{ij} = 0.35$ kJ·mol^{-1}. In detail, γ_i^S of component 1 (dashed line) and component 2 (solid line). Error bars with the uncertainty for T, $\sigma_T = 1.30$ K.

Based on the previous results, the non-ideal behavior of this mixture was evaluated. The SLE modeling of a system with solid phase non-ideality and miscibility requires that $z_i\,\gamma_i^S \neq 1.0$. Given the similarity of the two compounds and the results obtained above, for the modeling of the phase diagram it was assumed that the non-ideality of this mixture is only due to the solid phase, and the 2-suffix-

Margules equation was used for the description of the activity coefficient of the solid phase γ_i^S.

Figure 20 presents the phase diagram of such system comprising both *liquidus* and *solidus* lines. This γ_i model was chosen because even with just one single adjustable parameter, a_{ij}, the description of the experimental data is as accurate as obtained for the other systems. The calculated phase diagram shows a homogeneous azeotrope-type shape with a minimum point close to x_1 = 0.340 ([C_3C_1pyrr][PF_6]) mole fraction and a narrow biphasic region, *i.e.*, $x_i \cong z_i$. This profile is in agreement with a positive deviation from ideality[113], as depicted in detail in figure 20.

The forecast of this behavior with COSMO-RS failed, since it predicted an eutectic-like phase behavior instead of a solid-solution phase behavior.

4. Final Remarks

4.1. Conclusions

In this work, mixtures of mesothermal salts were prepared and their phase behavior were assessed by DSC and polarized optical microscopy, showing that novel ionic liquids can be prepared by simply mixing these salts and thus expanding their range of application. Moreover, based on the gathered data it was possible to conclude that, and in accordance with literature, most IL-IL or similar components mixtures have a quasi-ideal behavior. The results obtained also show the importance of considering the solid-solid transitions enthalpies and temperatures into the modeling of the phase diagrams since the solid-solid phase transitions presented by some of these components are far from negligible. The ideal liquid phase model was in good agreement with almost of the solid-liquid phase behavior measured, demonstrating therefore the capability of predicting their solid-liquid phase behavior based only on pure components properties, such as the melting temperature and enthalpies.

The non-ideality of the liquid phase behavior in some studied mixtures was also evaluated. In general, it was found that the differences in the cation alkyl chain length could contribute to a deviation from the ideal behavior. Also, the mixture between symmetric tetraalkylammoniums and phosphoniums, with a more pronounced aliphatic character, when mixed with other components constituted by heterocyclic aromatic and saturated cations, also leads to deviations from ideality.

The predictive ability of COSMO-RS was evaluated and compared with experimental data. COSMO-RS is capable of predicting the eutectic phase behavior and the deviations from ideality of systems composed of ionic liquid mixtures. This means that it can be used as a screening tool, by predicting their SLE phase behavior and their thermodynamics properties, in the design of new ionic liquids generated by mixing of ionic solids,. Moreover, COSMO-RS can be useful in the understanding of the main interactions occurring between the components in the mixtures and their contributions to the deviations on the ideal

behavior. This information allows to design new materials with outstanding characteristics based on the mixture of other materials.

Finally, an unique behavior was observed - a continuous solid solution by the formation of an alloy composed of $[C_3C_1pyrr][PF_6]$ and $[C_3C_1pip][PF_6]$. This was the first time that a mixture composed of two organic and short alkyl chain salts was reported, being this a rare phenomenon among organic compounds.

4.2. **Future work**

The possibilities of future work are immense. One possibility, and as a direct continuation of this work, is to extend the investigation carried out to mixtures composed of IL-IL with a common cation while varying the anion. This would allow the scanning of a much vaster range of liquid phase non-idealities.

Another possible approach is to determine the thermophysical properties of these mixtures in order to get a better characterization and understanding of their physicochemical characteristics. This type information will represent a large contribution on the knowledge of the major properties obtained by simply mixing ionic liquids.

To conclude, in this work, it was detected a lack of capability to predict high non-ideal systems, as solid solutions. Therefore, it would be interesting to develop an approach that could provide a deeper understanding of the influence of the solid-solid transitions and of the crystalline lattice in mixtures with a more complex solid-liquid phase behavior. Moreover, it would be relevant if one could integrate further parameters of pure components that could reflect important crystallographic properties with the thermodynamic properties, allowing therefore the prediction of more accurate high deviations to the non ideality on the phase behavior.

5. References

1. Annat, G.; Forsyth, M.; MacFarlane, D. R., Ionic Liquid Mixtures-Variations in Physical Properties and Their Origins in Molecular Structure. *J Phys Chem B* 2012, *116* (28), 8251-8258.

2. Kick, M.; Keil, P.; König, A., Solid–liquid phase diagram of the two Ionic Liquids EMIMCl and BMIMCl. *Fluid Phase Equilibr* 2013, *338* (0), 172-178.

3. Plechkova, N. V.; Seddon, K. R., Applications of ionic liquids in the chemical industry. *Chem Soc Rev* 2008, *37* (1), 123-150.

4. Niedermeyer, H.; Hallett, J. P.; Villar-Garcia, I. J.; Hunt, P. A.; Welton, T., Mixtures of ionic liquids. *Chem Soc Rev* 2012, *41* (23), 7780-7802.

5. Seddon, K. R., Ionic liquids for clean technology. *J Chem Technol Biot* 1997, *68* (4), 351-356.

6. Bonhote, P.; Dias, A. P.; Armand, M.; Papageorgiou, N.; Kalyanasundaram, K.; Gratzel, M., Hydrophobic, highly conductive ambient-temperature molten salts (vol 35, pg 1168, 1996). *Inorg Chem* 1998, *37* (1), 166-166.

7. Brennecke, J. F.; Maginn, E. J., Ionic liquids: Innovative fluids for chemical processing. *Aiche J* 2001, *47* (11), 2384-2389.

8. Walden, P., Ueber die Molekularegrosse und elektrische Leitfähigkeit einiger geschmolzenen Salze. *Bulletin de l'Académie Impériale des Sciences de St.-Pétersbourg* 1914, *8*, 405–422.

9. Graenacher, C., Cellulose solution. Google Patents: 1934.

10. Wang, H.; Gurau, G.; Rogers, R. D., Ionic liquid processing of cellulose. *Chem Soc Rev* 2012, *41* (4), 1519-1537.

11. Hurley, F. H.; WIer, T. P., Electrodeposition of Metals from Fused Quaternary Ammonium Salts. *J Electrochem Soc* 1951, *98* (5), 203-206.

12. Wilkes, J. S.; Zaworotko, M. J., Air and Water Stable 1-Ethyl-3-Methylimidazolium Based Ionic Liquids. *J Chem Soc Chem Comm* 1992, (13), 965-967.

13. Hallett, J. P.; Welton, T., Room-Temperature Ionic Liquids: Solvents for Synthesis and Catalysis. 2. *Chem Rev* 2011, *111* (5), 3508-3576.

14. Web of knowledge. http://www.webofknowledge.com/ (accessed 05-03-2014).

15. Freemantle, M., Designer solvents - Ionic liquids may boost clean technology development. *Chem Eng News* 1998, *76* (13), 32-37.

16. Harris, R. C. Physical Properties of Alcohol Based Deep Eutectic Solvents. Doctoral, University of Leicester, 2009.

17. Welton, T., Room-temperature ionic liquids. Solvents for synthesis and catalysis. *Chem Rev* 1999, *99* (8), 2071-2083.

18. Chatel, G.; Pereira, J. F. B.; Debbeti, V.; Wang, H.; Rogers, R. D., Mixing ionic liquids - "simple mixtures" or "double salts"? *Green Chem* 2014.

19. Long, J. X.; Guo, B.; Li, X. H.; Jiang, Y. B.; Wang, F. R.; Tsang, S. C.; Wang, L. F.; Yu, K. M. K., One step catalytic conversion of cellulose to sustainable chemicals utilizing cooperative ionic liquid pairs. *Green Chem* 2011, *13* (9), 2334-2338.

20. Freire, M. G.; Teles, A. R. R.; Ferreira, R. A. S.; Carlos, L. D.; Lopes-da-Silva, J. A.; Coutinho, J. A. P., Electrospun nanosized cellulose fibers using ionic liquids at room temperature. *Green Chem* 2011, *13* (11), 3173-3180.

21. Finotello, A.; Bara, J. E.; Narayan, S.; Camper, D.; Noble, R. D., Ideal gas solubilities and solubility selectivities in a binary mixture of room-temperature ionic liquids. *J Phys Chem B* 2008, *112* (8), 2335-2339.

22. Ferrari, S.; Quartarone, E.; Mustarelli, P.; Magistris, A.; Protti, S.; Lazzaroni, S.; Fagnoni, M.; Albini, A., A binary ionic liquid system composed of N-methoxyethyl-N-methylpyrrolidinium bis(trifluoromethanesulfonyl)-imide and lithium bis(trifluoromethanesulfonyl)imide: A new promising electrolyte for lithium batteries. *J Power Sources* 2009, *194* (1), 45-50.

23. Hao, F.; Lin, H.; Liu, Y. Z.; Li, J. B., Anionic structure-dependent photoelectrochemical responses of dye-sensitized solar cells based on a binary ionic liquid electrolyte. *Phys Chem Chem Phys* 2011, *13* (14), 6416-6422.

24. Zistler, M.; Wachter, P.; Schreiner, C.; Fleischmann, M.; Gerhard, D.; Wasserscheid, P.; Hinsch, A.; Goresa, H. J., Temperature dependent impedance analysis of binary ionic liquid electrolytes for dye-sensitized solar cells. *J Electrochem Soc* 2007, *154* (9), B925-B930.

25. Khosropour, A. R.; Mohammadpoor-Baltork, I.; Kiani, F., Green, new and efficient tandem oxidation and conversion of aryl alcohols to 2,4,6-triarylpyridines promoted by [HMIm]NO_3-[BMIm]BF_4 as a binary ionic liquid. *Cr Chim* 2011, *14* (5), 441-445.

26. Baltazar, Q. Q.; Leininger, S. K.; Anderson, J. L., Binary ionic liquid mixtures as gas chromatography stationary phases for improving the separation selectivity of alcohols and aromatic compounds. *J Chromatogr A* 2008, *1182* (1), 119-127.

27. Ochedzan-Siodlak, W.; Dziubek, K., Improvement of biphasic polymerization by application of binary ionic liquid mixture. *Chem Eng Process* 2013, *72*, 74-81.

28. Larriba, M.; Navarro, P.; García, J.; Rodríguez, F., Liquid–liquid extraction of toluene from n-heptane by {[emim][TCM]+[emim][DCA]} binary ionic liquid mixtures. *Fluid Phase Equilibr* 2014, *364* (0), 48-54.

29. Choi, S.-A.; Oh, Y.-K.; Jeong, M.-J.; Kim, S. W.; Lee, J.-S.; Park, J.-Y., Effects of ionic liquid mixtures on lipid extraction from Chlorella vulgaris. *Renewable Energy* 2014, *65* (0), 169-174.

30. Pinto, A. M.; Rodríguez, H.; Colón, Y. J.; Arce, A.; Soto, A., Absorption of Carbon Dioxide in Two Binary Mixtures of Ionic Liquids. *Ind Eng Chem Res* 2013, *52* (17), 5975-5984.

31. Tome, L. C.; Patinha, D. J. S.; Freire, C. S. R.; Rebelo, L. P. N.; Marrucho, I. M., CO2 separation applying ionic liquid mixtures: the effect of mixing different anions on gas permeation through supported ionic liquid membranes. *Rsc Adv* 2013, *3* (30), 12220-12229.

32. Brussel, M.; Brehm, M.; Voigt, T.; Kirchner, B., Ab initio molecular dynamics simulations of a binary system of ionic liquids. *Phys Chem Chem Phys* 2011, *13* (30), 13617-13620.

33. Shimizu, K.; Tariq, M.; Rebelo, L. P. N.; Lopes, J. N. C., Binary mixtures of ionic liquids with a common ion revisited: A molecular dynamics simulation study. *J Mol Liq* 2010, *153* (1), 52-56.

34. Brussel, M.; Brehm, M.; Pensado, A. S.; Malberg, F.; Ramzan, M.; Stark, A.; Kirchner, B., On the ideality of binary mixtures of ionic liquids. *Phys Chem Chem Phys* 2012, *14* (38), 13204-13215.

35. Navia, P.; Troncoso, J.; Romani, L., Excess magnitudes for ionic liquid binary mixtures with a common ion. *J Chem Eng Data* 2007, *52* (4), 1369-1374.

36. Stoppa, A.; Buchner, R.; Hefter, G., How ideal are binary mixtures of room-temperature ionic liquids? *J Mol Liq* 2010, *153* (1), 46-51.

37. Oliveira, M. B.; Dominguez-Perez, M.; Freire, M. G.; Llovell, F.; Cabeza, O.; Lopes-da-Silva, J. A.; Vega, L. F.; Coutinho, J. A. P., Surface Tension of Binary Mixtures of 1-Alkyl-3-methylimidazolium Bis(trifluoromethylsulfonyl)imide Ionic Liquids: Experimental Measurements and Soft-SAFT Modeling. *J Phys Chem B* 2012, *116* (40), 12133-12141.

38. Fox, E. T.; Paillard, E.; Borodin, O.; Henderson, W. A., Physicochemical Properties of Binary Ionic Liquid-Aprotic Solvent Electrolyte Mixtures. *J Phys Chem C* 2013, *117* (1), 78-84.

39. Oliveira, M. B.; Dominguez-Perez, M.; Cabeza, O.; Lopes-da-Silva, J. A.; Freire, M. G.; Coutinho, J. A. P., Surface tensions of binary mixtures of ionic

liquids with bis(trifluoromethylsulfonyl) imide as the common anion. *J Chem Thermodyn* 2013, *64*, 22-27.

40. Song, D.; Chen, J., Density and Viscosity Data for Mixtures of Ionic Liquids with a Common Anion. *Journal of Chemical & Engineering Data* 2014, *59* (2), 257-262.

41. Annat, G.; MacFarlane, D. R.; Forsyth, M., Transport properties in ionic liquids and ionic liquid mixtures: The challenges of NMR pulsed field gradient diffusion measurements. *J Phys Chem B* 2007, *111* (30), 9018-9024.

42. Lopes, J. N. C.; Cordeiro, T. C.; Esperanca, J. M. S. S.; Guedes, H. J. R.; Huq, S.; Rebelo, L. P. N.; Seddon, K. R., Deviations from ideality in mixtures of two ionic liquids containing a common ion. *J Phys Chem B* 2005, *109* (8), 3519-3525.

43. Earle, M. J.; Esperanca, J. M. S. S.; Gilea, M. A.; Lopes, J. N. C.; Rebelo, L. P. N.; Magee, J. W.; Seddon, K. R.; Widegren, J. A., The distillation and volatility of ionic liquids. *Nature* 2006, *439* (7078), 831-834.

44. Widegren, J. A.; Wang, Y. M.; Henderson, W. A.; Magee, J. W., Relative volatilities of ionic liquids by vacuum distillation of mixtures. *J Phys Chem B* 2007, *111* (30), 8959-8964.

45. Wasserscheid, P., Chemistry - Volatile times for ionic liquids. *Nature* 2006, *439* (7078), 797-797.

46. Every, H.; Bishop, A. G.; Forsyth, M.; MacFarlane, D. R., Ion diffusion in molten salt mixtures. *Electrochim Acta* 2000, *45* (8-9), 1279-1284.

47. Nakajima, K.; Miyashita, M.; Suzuki, M.; Kimura, K., Surface structures of binary mixtures of imidazolium-based ionic liquids using high-resolution Rutherford backscattering spectroscopy and time of flight secondary ion mass spectroscopy. *J Chem Phys* 2013, *139* (22).

48. Greaves, T. L.; Kennedy, D. F.; Kirby, N.; Drummond, C. J., Nanostructure changes in protic ionic liquids (PILs) through adding solutes and mixing PILs. *Phys Chem Chem Phys* 2011, *13* (30), 13501-13509.

49. Fletcher, K. A.; Baker, S. N.; Baker, G. A.; Pandey, S., Probing solute and solvent interactions within binary ionic liquid mixtures. *New J Chem* 2003, *27* (12), 1706-1712.

50. Arce, A.; Earle, M. J.; Katdare, S. P.; Rodriguez, H.; Seddon, K. R., Phase equilibria of mixtures of mutually immiscible ionic liquids. *Fluid Phase Equilibr* 2007, *261* (1-2), 427-433.

51. Omar, S.; Lemus, J.; Ruiz, E.; Ferro, V. R.; Ortega, J.; Palomar, J., Ionic Liquid Mixtures—An Analysis of Their Mutual Miscibility. *The Journal of Physical Chemistry B* 2014.

52. Xiao, D.; Rajian, J. R.; Li, S. F.; Bartsch, R. A.; Quitevis, E. L., Additivity in the optical Kerr effect spectra of binary ionic liquid mixtures: Implications for nanostructural organization. *J Phys Chem B* 2006, *110* (33), 16174-16178.

53. Henderson, W. A.; Passerini, S., Phase behavior of ionic liquid-LiX mixtures: Pyrrolidinium cations and TFSI- anions. *Chem Mater* 2004, *16* (15), 2881-2885.

54. Kunze, M.; Jeong, S.; Paillard, E.; Winter, M.; Passerini, S., Melting Behavior of Pyrrolidinium-Based Ionic Liquids and Their Binary Mixtures. *J Phys Chem C* 2010, *114* (28), 12364-12369.

55. Fannin, A. A.; Floreani, D. A.; King, L. A.; Landers, J. S.; Piersma, B. J.; Stech, D. J.; Vaughn, R. L.; Wilkes, J. S.; Williams, J. L., Properties of 1,3-Dialkylimidazolium Chloride Aluminum-Chloride Ionic Liquids .2. Phase-Transitions, Densities, Electrical Conductivities, and Viscosities. *J Phys Chem-Us* 1984, *88* (12), 2614-2621.

56. Montanino, M.; Moreno, M.; Alessandrini, F.; Appetecchi, G. B.; Passerini, S.; Zhou, Q.; Henderson, W. A., Physical and electrochemical properties of binary

ionic liquid mixtures: (1-x) $PYR_{14}TFSI^-$(x) PYR14IM14. *Electrochim Acta* 2012, *60*, 163-169.

57. Zhou, Q.; Fitzgerald, K.; Boyle, P. D.; Henderson, W. A., Phase Behavior and Crystalline Phases of Ionic Liquid-Lithium Salt Mixtures with 1-Alkyl-3-methylimidazolium Salts. *Chem Mater* 2010, *22* (3), 1203-1208.

58. Zhou, Q.; Henderson, W. A.; Appetecchi, G. B.; Passerini, S., Phase Behavior and Thermal Properties of Ternary Ionic Liquid-Lithium Salt (IL-IL-LiX) Electrolytes. *J Phys Chem C* 2010, *114* (13), 6201-6204.

59. Hayamizu, K.; Aihara, Y.; Nakagawa, H.; Nukuda, T.; Price, W. S., Ionic conduction and ion diffusion in binary room-temperature ionic liquids composed of [emim][BF_4] and $LiBF_4$. *J Phys Chem B* 2004, *108* (50), 19527-19532.

60. Scheers, J.; Pitawala, J.; Thebault, F.; Kim, J. K.; Ahn, J. H.; Matic, A.; Johansson, P.; Jacobsson, P., Ionic liquids and oligomer electrolytes based on the B(CN)(4)(-) anion; ion association, physical and electrochemical propertiesw. *Phys Chem Chem Phys* 2011, *13* (33), 14953-14959.

61. Bayley, P. M.; Best, A. S.; MacFarlane, D. R.; Forsyth, M., Transport Properties and Phase Behaviour in Binary and Ternary Ionic Liquid Electrolyte Systems of Interest in Lithium Batteries. *Chemphyschem* 2011, *12* (4), 823-827.

62. Pavlechko, Y. U.; Kabo, G. Y., Heat capacity and phase transitions of a mixture of ionic liquids [$C_{(2)}$mim]NTf(2)+[$C_{(6)}$mim]NTf(2). *Russ J Phys Chem a+* 2008, *82* (8), 1412-1414.

63. Sun, J.; Forsyth, M.; MacFarlane, D. R., Room-temperature molten salts based on the quaternary ammonium ion. *J Phys Chem B* 1998, *102* (44), 8858-8864.

64. Arce, A.; Earle, M. J.; Katdare, S. P.; Rodriguez, H.; Seddon, K. R., Mutually immiscible ionic liquids. *Chem Commun* 2006, (24), 2548-2550.

65. Kagimoto, J.; Nakamura, N.; Kato, T.; Ohno, H., Novel thermotropic gels composed of only ions. *Chem Commun* 2009, (17), 2405-2407.

66. Apperley, D. C.; Hardacre, C.; Licence, P.; Murphy, R. W.; Plechkova, N. V.; Seddon, K. R.; Srinivasan, G.; Swadzba-Kwasny, M.; Villar-Garcia, I. J., Speciation of chloroindate(III) ionic liquids. *Dalton T* 2010, *39* (37), 8679-8687.

67. Fox, E. T.; Weaver, J. E. F.; Henderson, W. A., Tuning Binary Ionic Liquid Mixtures: Linking Alkyl Chain Length to Phase Behavior and Ionic Conductivity. *J Phys Chem C* 2012, *116* (8), 5271-5275.

68. Gamsjäger, H.; Lorimer, J. W.; Scharlin, P.; Shaw, D. G., Glossary of terms related to solubility (IUPAC Recommendations 2008). *Pure Appl Chem* 2008, *80* (2), 233-276.

69. Abbott, A. P.; Barron, J. C.; Ryder, K. S.; Wilson, D., Eutectic-based ionic liquids with metal-containing anions and cations. *Chem-Eur J* 2007, *13* (22), 6495-6501.

70. Zhang, Q. H.; Vigier, K. D.; Royer, S.; Jerome, F., Deep eutectic solvents: syntheses, properties and applications. *Chem Soc Rev* 2012, *41* (21), 7108-7146.

71. Russ, C.; Konig, B., Low melting mixtures in organic synthesis - an alternative to ionic liquids? *Green Chem* 2012, *14* (11), 2969-2982.

72. Francisco, M.; van den Bruinhorst, A.; Kroon, M. C., Low-Transition-Temperature Mixtures (LTTMs): A New Generation of Designer Solvents. *Angew Chem Int Edit* 2013, *52* (11), 3074-3085.

73. M. Gordon, C.; D. Holbrey, J.; R. Kennedy, A.; R. Seddon, K., Ionic liquid crystals: hexafluorophosphate salts. *J Mater Chem* 1998, *8* (12), 2627-2636.

74. Wang, M.; Pan, X.; Xiao, S.; Zhang, C.; Li, W.; Dai, S., Regulating mesogenic properties of ionic liquid crystals by preparing binary or multi-component systems. *J Mater Chem* 2012, *22* (5), 2299-2305.

75. Atkins, P.; De Paula, J., *Physical Chemistry*. Seventh ed.; Oxford University Press: 2002.

76. Castejon, H. J.; Lashock, R. J., Mixtures of ionic liquids with similar molar volumes form regular solutions and obey the cross-square rules for electrolyte mixtures. *J Mol Liq* 2012, *167*, 1-4.

77. Kleppa, O. J.; McCarty, F. G., Thermochemistry of charge-unsymmetrical binary fused halide systems .2. mixtures of magnesium chloride with alkali chlorides and with silver chloride. *J Phys Chem-Us* 1966, *70* (4), 1249-&.

78. Lumsden, J., *Thermodynamics of molten salt mixtures*. London, 1966; p 352.

79. Kleppa, O. J.; Hersh, L. S., Heats of mixing in liquid alkali nitrate systems. *J Chem Phys* 1961, *34* (2), 351-&.

80. Kleppa, O. J.; Meschel, S. V., Thermochemistry of anion mixtures in simple fused salt systems .1. Solutions of monovalent chlorides and bromides in corresponding nitrates. *J Phys Chem-Us* 1963, *67* (3), 668-&.

81. Kleppa, O. J., Solution Chemistry of Simple Fused Salts. *Annual Review of Physical Chemistry* 1965, *16*, 187-&.

82. Prausnitz, J. M. L., R.N.; Azevedo,E.G., *Molecular thermodynamics of fluid-phase equilibria*. Second ed.; New Jersey, 1986.

83. Prausnitz, J. M.; Lichtenthaler, R. N.; Azevedo, E. G., *Molecular thermodynamics of fluid-phase equilibria*. 2nd ed.; Prentice-Hall: New Jersey, 1986.

84. Coutinho, J. A. P.; Andersen, S. I.; Stenby, E. H., Evaluation of activity coefficient models in prediction of alkane solid-liquid equilibria. *Fluid Phase Equilibr* 1995, *103* (1), 23-39.

85. Reid, R. C.; Prausnitz, J. M.; Pouling, B. E., *The properties of gases and liquids*. 4th ed.; McGraw-Hill: New York, 1987.

86. Klamt, A., Conductor-like screening model for real solvents: A new approach to the quantitative calculation of solvation phenomena. *J Phys Chem-Us* 1995, *99* (7), 2224-2235.

87. Klamt, A.; Eckert, F., COSMO-RS: a novel and efficient method for the a priori prediction of thermophysical data of liquids. *Fluid Phase Equilibr* 2000, *172* (1), 43-72.

88. Klamt, A.; Jonas, V.; Bürger, T.; Lohrenz, J. C. W., Refinement and parametrization of COSMO-RS. *J Phys Chem A* 1998, *102* (26), 5074-5085.

89. Freire, M. G.; Santos, L. M. N. B. F.; Marrucho, I. M.; Coutinho, J. A. P., Evaluation of COSMO-RS for the prediction of LLE and VLE of alcohols plus ionic liquids. *Fluid Phase Equilibr* 2007, *255* (2), 167-178.

90. Schäfer, A.; Klamt, A.; Sattel, D.; Lohrenz, J. C. W.; Eckert, F., COSMO implementation in TURBOMOLE: Extension of an efficient quantum chemical code towards liquid systems. *Phys. Chem. Chem. Phys.* 2000, *2* (10), 2187-2193.

91. Schäfer, A.; Huber, C.; Ahlrichs, R., Fully optimized contracted Gaussian Basis Sets of Triple Zeta Valence quality for atoms Li to Kr. *J. Chem. Phys.* 1994, *100* (8), 5829-5835.

92. Ferreira, A. R.; Freire, M. G.; Ribeiro, J. C.; Lopes, F. M.; Crespo, J. G.; Coutinho, J. A. P., Ionic liquids for thiols desulfurization: Experimental liquid–liquid equilibrium and COSMO-RS description. *Fuel* 2014, *128* (0), 314-329.

93. Freire, M. G.; Ventura, S. P. M.; Santos, L. M. N. B. F.; Marrucho, I. M.; Coutinho, J. A. P., Evaluation of COSMO-RS for the prediction of LLE and VLE of water and ionic liquids binary systems. *Fluid Phase Equilibr* 2008, *268* (1-2), 74-84.

94. Diedenhofen, M.; Klamt, A., COSMO-RS as a tool for property prediction of IL mixtures-A review. *Fluid Phase Equilibr* 2010, *294* (1-2), 31-38.

95. Verma, N. R.; Gopal, G.; Anantharaj, R.; Banerjee, T., (Solid plus liquid) equilibria predictions of ionic liquid containing systems using COSMO-RS. *The Journal of Chemical Thermodynamics* 2012, *48* (0), 246-253.

96. Educational Astronomical Photography and Video. http://astrophotovideo.wordpress.com/adapting-a-webcam-to-a-telescope/.

97. Westen, M. v. Science4all. http://science4all.nl/.

98. D'Amelia, R. P.; Nirode, W. F.; Franks, T., Introduction of differential scanning calorimetry (DSC) in a general chemistry laboratory course: Determination of molar mass by freezing point depression. *Abstr Pap Am Chem S* 2005, *230*, U802-U802.

99. Sheldrick, G., A short history of SHELX. *Acta Crystallographica Section A* 2008, *64* (1), 112-122.

100. Lopez-Martin, I.; Burello, E.; Davey, P. N.; Seddon, K. R.; Rothenberg, G., Anion and cation effects on imidazolium salt melting points: A descriptor modelling study. *Chemphyschem* 2007, *8* (5), 690-695.

101. Rocha, M. A. A.; Ribeiro, F. M. S.; Ferreira, A. I. M. C. L.; Coutinho, J. A. P.; Santos, L. M. N. B. F., Thermophysical properties of $[C(_{N-1})C(_{1})im][PF_6]$ ionic liquids. *J Mol Liq* 2013, *188*, 196-202.

102. Rocha, M. A. A.; Coutinho, J. A. P.; Santos, L. M. N. B. F., Cation Symmetry effect on the Volatility of Ionic Liquids. *J Phys Chem B* 2012, *116* (35), 10922-10927.

103. Rocha, M. A. A.; Lima, C. F. R. A. C.; Gomes, L. g. R.; Schröder, B.; Coutinho, J. o. A. P.; Marrucho, I. M.; Esperança, J. M. S. S.; Rebelo, L. s. P. N.; Shimizu, K.; Lopes, J. N. C.; Santos, L. s. M. N. B. F., High-Accuracy Vapor Pressure Data of the Extended $[C_nC_1im][Ntf_2]$ Ionic Liquid Series: Trend Changes and Structural Shifts. *The Journal of Physical Chemistry B* 2011, *115* (37), 10919-10926.

104. Gordon, J. E.; Subbarao, G. N., Fused Organic Salts .8. Properties of Molten Straight-Chain Isomers of Tetra-Normal-Pentylammonium Salts. *J Am Chem Soc* 1978, *100* (24), 7445-7454.

105. Golding, J.; Hamid, N.; MacFarlane, D. R.; Forsyth, M.; Forsyth, C.; Collins, C.; Huang, J., N-methyl-N-alkylpyrrolidinium hexafluorophosphate salts: Novel molten salts and plastic crystal phases. *Chem Mater* 2001, *13* (2), 558-564.

106. Pringle, J. M.; Adebahr, J.; MacFarlane, D. R.; Forsyth, M., Unusual phase behaviour of the organic ionic plastic crystal N,N-dimethylpyrrolidinium tetrafluoroborate. *Phys Chem Chem Phys* 2010, *12* (26), 7234-7240.

107. Ono, H.; Ishimaru, S. I.; Ikeda, R.; Ishida, H., Ionic plastic phase in piperidinium hexafluorophosphate studied by solid NMR, X-Ray diffraction, and thermal measurements. *Berichte der Bunsengesellschaft für physikalische Chemie* 1998, *102* (4), 650-655.

108. Timmermans, J., Plastic crystals: A historical review. *Journal of Physics and Chemistry of Solids* 1961, *18* (1), 1-8.

109. MacFarlane, D. R.; Meakin, P.; Sun, J.; Amini, N.; Forsyth, M., Pyrrolidinium imides: A new family of molten salts and conductive plastic crystal phases. *J Phys Chem B* 1999, *103* (20), 4164-4170.

110. Yang, M.; Mallick, B.; Mudring, A. V., On the Mesophase Formation of 1,3-Dialkylimidazolium Ionic Liquids. *Cryst Growth Des* 2013, *13* (7), 3068-3077.

111. Costa, M. C.; Rolemberg, M. P.; Boros, L. A. D.; Krahenbuhl, M. A.; de Oliveira, M. G.; Meirelles, A. J. A., Solid-liquid equilibrium of binary fatty acid mixtures. *J Chem Eng Data* 2007, *52* (1), 30-36.

112. Maximo, G. J.; Costa, M. C.; Meirelles, A. J. A., Solid-liquid equilibrium of triolein with fatty alcohols. *Braz J Chem Eng* 2013, *30* (1), 33-43.

113. Ricci, J. E., *The Phase Rule and Heterogeneous Equilibrium*. Dover Publications: New York, 1966.

6. Appendix

6.1. Appendix A – Powder X-Ray Diffraction data for $[C_3C_1pip][PF_6]$

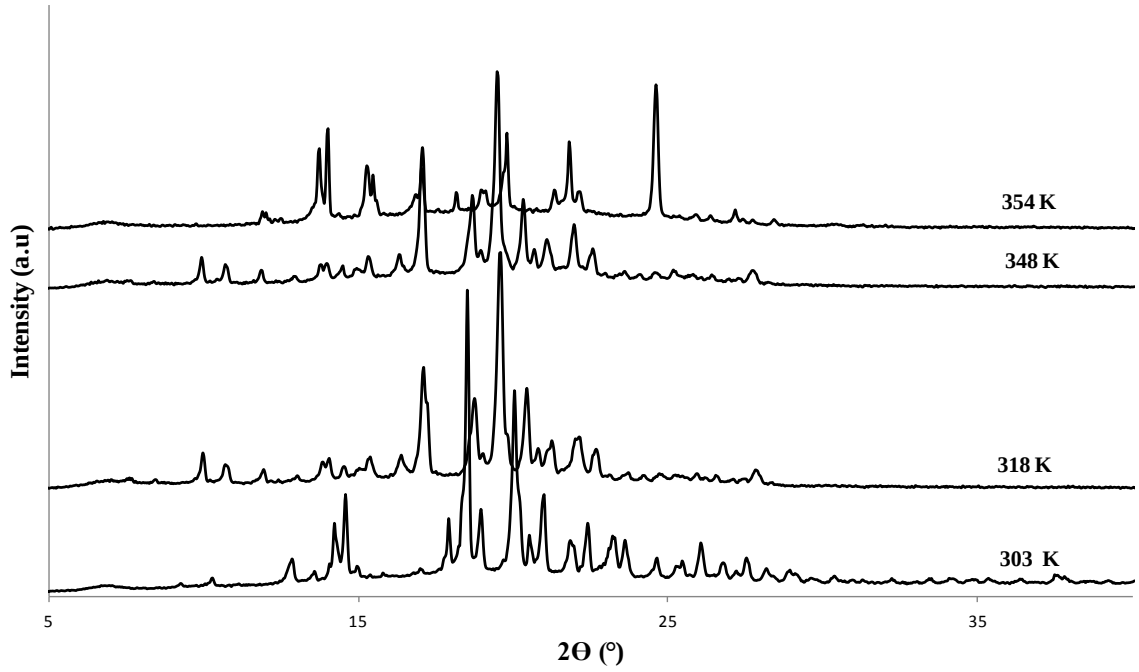

Figure A 1 - Powder XRD patterns from pure $[C_3C_1pip][PF_6]$ at different temperatures (T = 303 K, T = 318 K, T = 348 K and T= 354 K) illustrating the pattern shifts on the two S-S transitions.

6.2. Appendix B – Experimental data of binary mixtures

Table B 1 - Experimental solid-liquid equilibrium data for the binary mixtures of ILs, in mole fraction *x*, melting temperature *T*, and at a pressure *p* = 102.0 kPa [a].

[C_3C_1im][PF_6] (1) + [C_3C_1py][PF_6] (2)			[C_3C_1im][PF_6] (1) + [C_3C_1pyrr][PF_6] (2)			[C_3C_1im][PF_6] (1) + [C_3C_1pip][PF_6] (2)			[C_3C_1im][PF_6] (1) + [$C_{12}C_1$im][PF_6] (2)			[C_3C_1pyrr][PF_6] (1) + [C_3C_1pip][PF_6] (2)		
x_1	T / K	Solid phase	x_1	T / K	Solid phase	x_1	T / K	Solid phase	x_1	T / K	Solid phase	x_1	T / K	Solid phase
0.000	312.55	2	0.000	384.65	2	0.000	370.65	2	0.000	326.95	2	0.000	370.65	2
0.100	306.65	2	0.101	357.05	2	0.099	356.85	2	0.104	324.75	2	0.100	369.95	1 + 2
0.201	296.15	2	0.200	340.05	2	0.200	338.95	2	0.209	322.65	2	0.200	369.35	1 + 2
0.301	290.15	2	0.300	324.55	2	0.300	323.65	2	0.303	320.25	2	0.301	368.55	1 + 2
0.398	285.35	2	0.401	308.15	2	0.400	303.75	2	0.397	317.45	2	0.399	369.15	1 + 2
0.502	281.45	1	0.501	283.15	2	0.499	295.65	2	0.504	314.65	2	0.500	369.55	1 + 2
0.600	286.35	1	0.601	285.15	1	0.600	286.45	2	0.603	311.35	2	0.600	369.65	1 + 2
0.700	296.15	1	0.699	289.45	1	0.699	293.55	1	0.698	306.05	2	0.701	371.85	1 + 2
0.800	301.45	1	0.800	300.65	1	0.799	298.55	1	0.797	299.95	2	0.798	375.15	1 + 2
0.900	305.55	1	0.900	303.15	1	0.900	307.05	1	0.849	297.85	2	0.900	381.60	1 + 2
1.000	312.15	1	1.000	312.15	1	1.000	312.15	1	0.906	298.15	1	1.000	384.65	1
									0.953	305.65	1			
									1.000	312.15	1			

[a] Uncertainties for mole fraction, temperature and pressure are ± 0.001, ± 1.30 K and ± 0.5 kPa, respectively.

Table B 2 - Experimental solid-liquid equilibrium data of the binary mixtures of ILs for mole fraction x, melting temperature T and pressure p = 102.0 kPa [a]. (continuation)

$[C_3C_1pyrr][PF_6]$ (1) + $[C_3C_1py][PF_6]$ (2)			$[C_3C_1py][PF_6]$ (1) + $[C_3C_1pip][PF_6]$ (2)			$[C_3C_1im][PF_6]$ (1) + $[P_{4,4,4,4}][PF_6]$ (2)			$[C_3C_1im][PF_6]$ (1) + $[N_{4,4,4,4}][PF_6]$ (2)		
x_1	T / K	Solid phase	x_1	T / K	Solid phase	x_1	T / K	Solid phase	x_1	T / K	Solid phase
0.000	312.55	2	0.000	370.65	2	0.000	498.60	2	0.000	524.30	2
0.100	306.55	2	0.105	354.85	2	0.750	392.95	2	0.809	392.35	2
0.200	294.65	2	0.311	328.65	2	0.800	382.15	2	0.855	384.25	2
0.300	291.35	2	0.401	318.15	2	0.900	352.65	2	0.904	366.25	2
0.400	284.65	2	0.499	306.15	2	0.950	308.15	2	0.955	338.05	2
0.500	291.45	1	0.600	285.15	2	1.000	312.15	1	1.000	312.15	1
0.599	313.15	1	0.701	289.15	1						
0.700	333.35	1	0.800	303.15	1						
0.800	342.15	1	0.900	307.15	1						
0.899	356.85	1	1.000	312.55	1						
1.000	384.65	1									

[a] Uncertainties for mole fraction, temperature and pressure are ± 0.001, ± 1.30 K and ± 0.5 kPa, respectively

6.3. Appendix C – COSMO-RS Excess enthalpies

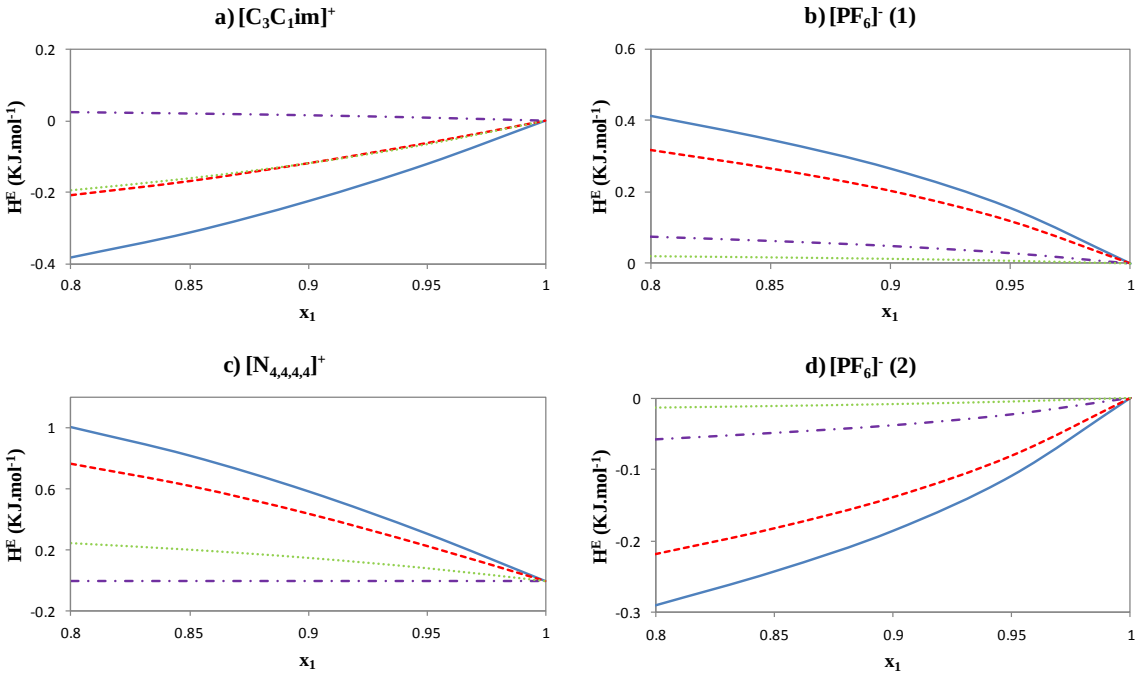

Figure C 1 – Excess enthalpies forecasted by COSMO-RS for the system $[N_{4,4,4,4}][C_3C_1im][PF_6]$. The excess enthalpies were calculated from the contributions of each individual constituent: a) $[C_3C_1im]^+$, b) $[PF_6]^-$ (1 - coupled with imidazolium based cation), c) $[N_{4,4,4,4}]^+$, d) $[PF_6]^-$ (2 - coupled with ammonium based cation). The comparison was made between the total excess enthalpy (blue, full line) and the different interactions contributions, *i.e.*, (red, dashed line) for electrostatic interactions, (purple, dotted and dashed line) for H-bonding interactions, and (green, dotted line) for van der Waals forces.

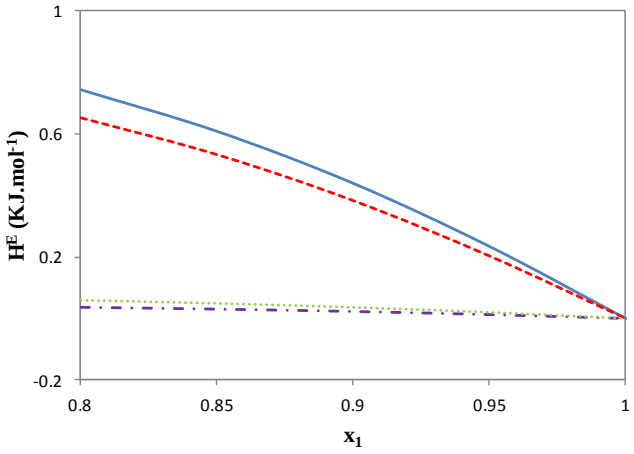

Figure C 2 - Global excess enthalpies calculated by COSMO-RS for the system $[C_3C_1im][N_{4,4,4,4}][PF_6]$. The comparison was made between the total excess enthalpy (blue, full line) and the different interactions contributions, *i.e.*, (red, dashed line) for electrostatic interactions, (purple, dotted and dashed line) for H-bonding interactions, and (green, dotted line) for van der Waals forces.

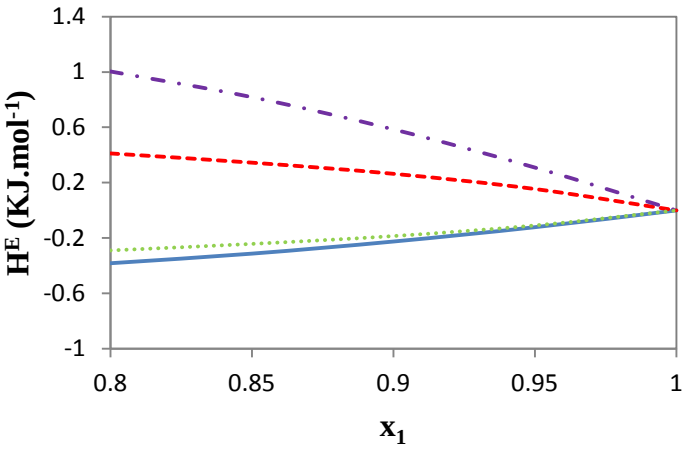

Figure C 3 - Individual ions' total contributions for total excess enthalpy for $[C_3C_1im][N_{4,4,4,4}][PF_6]$ calculated by COSMO-RS. The comparison was made between the total excess enthalpy for $[C_3C_1im]^+$ (blue, full line)], for $[PF_6]^-$ (1- coupled with imidazolium based cation) (red, dashed line), $[N_{4,4,4,4}]^+$(purple, dotted and dashed line) and $[PF_6]^-$ (2 - coupled with ammonium based cation) (green, dotted line).

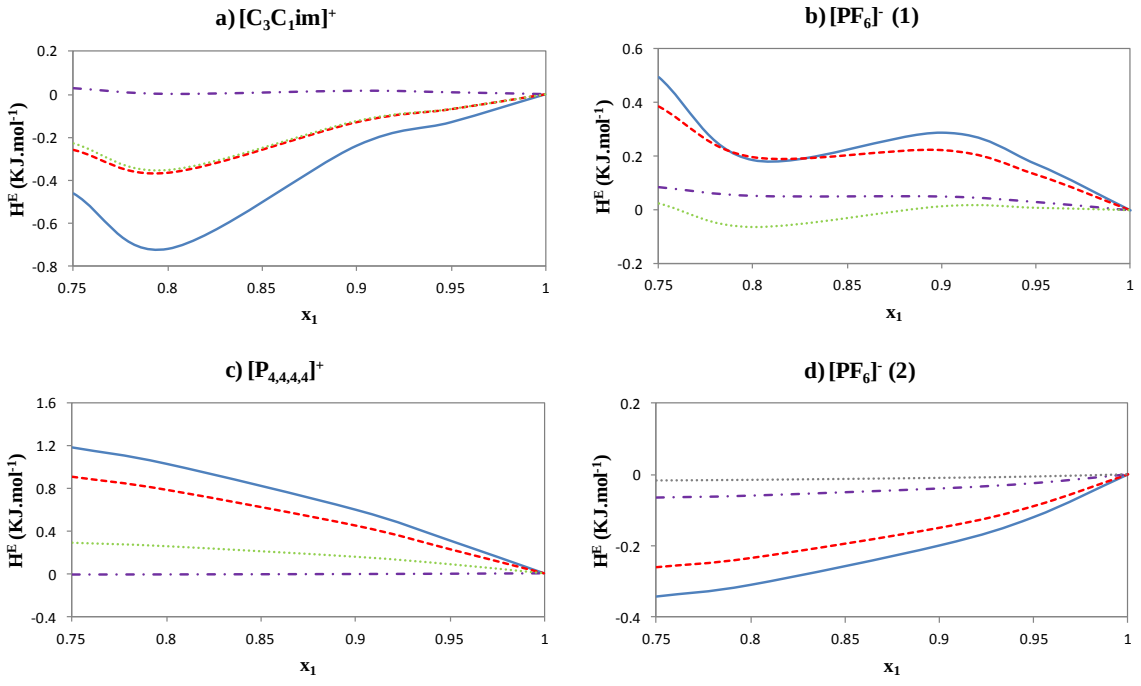

Figure C 4 - Excess enthalpies forecasted by COSMO-RS for the system $[P_{4,4,4,4}][PF_6]$ $[C_3C_1im][PF_6]$. The excess enthalpies were calculated from the contributions of each individual constituent: a) $[C_3C_1im]^+$, b) $[PF_6]^-$(1- coupled with imidazolium based cation), c) $[P_{4,4,4,4}]^+$, d) $[PF_6]^-$ (2 - coupled with ammonium based cation). The comparison was made between the total excess enthalpy (blue, full line) and the different interactions contributions, *i.e.*, (red, dashed line) for electrostatic interactions, (purple, dotted and dashed line) for H-bonding interactions, and (green, dotted line) for van der Waals forces.

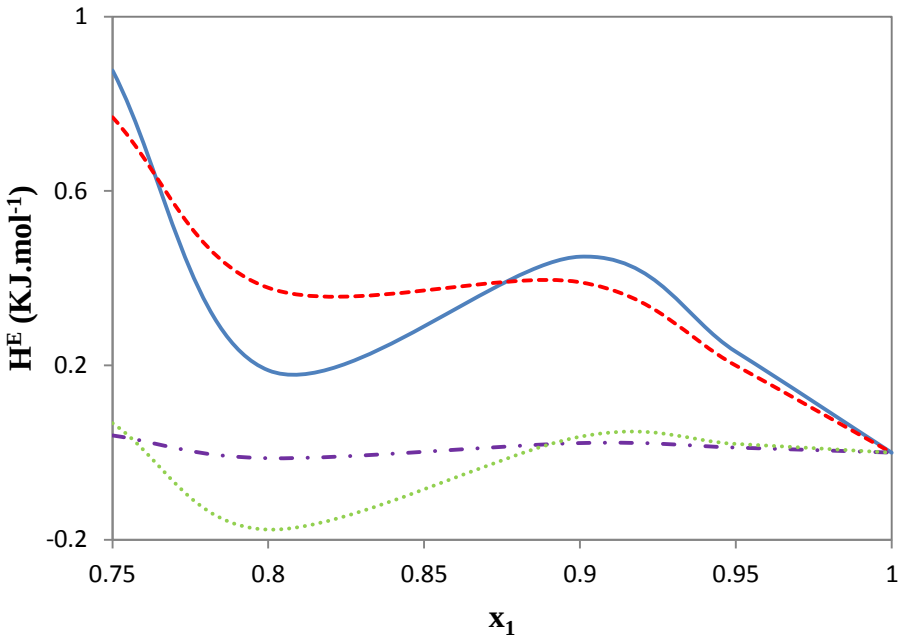

Figure C 5 - Global excess enthalpies calculated by COSMO-RS for the system $[C_3C_1im][P_{4,4,4,4}][PF_6]$. The comparison was made between the total excess enthalpy (blue, full line) and the different interactions contributions, *i.e.*, (red, dashed line) for electrostatic interactions, (purple, dotted and dashed line) for H-bonding interactions, and (green, dotted line) for van der Waals forces.

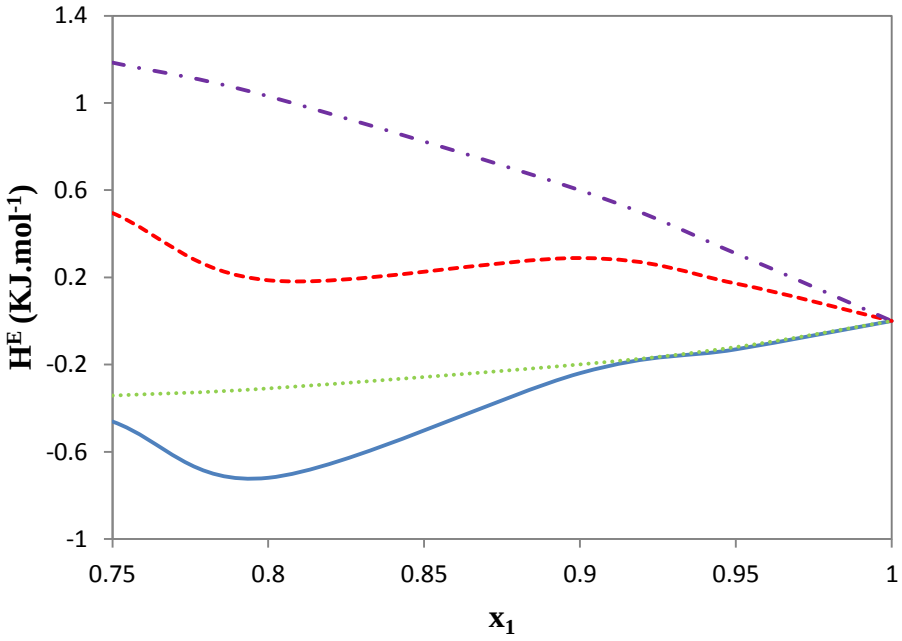

Figure C 6 - Individual ions' total contributions for total excess enthalpy for $[C_3C_1im][P_{4,4,4,4}][PF_6]$ calculated by COSMO-RS. The comparison was made between the total excess enthalpy for $[C_3C_1im]^+$ (blue, full line)], for $[PF_6]^-$ (1- coupled with imidazolium based cation) (red, dashed line), $[P_{4,4,4,4}]^+$(purple, dotted and dashed line) and $[PF_6]^-$ (2 - coupled with ammonium based cation) (green, dotted line).

7. List of publications

Co-author in:

- Maximo, G. J.; Santos, R. J. B. N.; Lopes-da-Silva, J. A.; Costa, M. C.; Meirelles, A. J. A.; Coutinho, J. A. P., Lipidic Protic Ionic Liquid Crystals. *Acs Sustain Chem Eng* **2013,** *2* (4), 672-682.

- Maximo, G. J.; Santos, R. J. B. N.; Esperança, J. M. S. S.; Costa, M. C.; Meirelles, A. J. A.; Freire; M. G.; Coutinho, J. A. P., Generating ionic liquids from ionic solids: An investigation on the melting behavior of binary mixtures of ionic liquids, Crystal Growth & Design, 2014, accepted for publication.